coatings

MDPI

Article

Bridge Structure Damage Identification Based on Dynamic Characteristics

Yunkai Zhang [1,2,*], Xixue Tan [1,2], Guohua Li [1], Jun Dong [1,2], Jingyi Guo [1] and Fanyue Liu [1]

[1] School of Civil and Transportation Engineering, Beijing University of Civil Engineering and Architecture, Beijing 102616, China; 201802020414@stu.bucea.edu.cn (X.T.); liguohua@bucea.edu.cn (G.L.); dongjun@bucea.edu.cn (J.D.); 201802030120@stu.bucea.edu.cn (J.G.); 201802020125@stu.bucea.edu.cn (F.L.)
[2] Yunchuang Intelligent Testing Technology Institute, Beijing University of Civil Engineering and Architecture, Beijing 102616, China
* Correspondence: 201802040124@stu.bucea.edu.cn

Abstract: With the increasing traffic volume and years of usage during the operation process, a bridge structure will experience aging and damage to different degrees, leading to the decline in bridge reliability and seriously affecting its operation safety. In this study, the bridge was abstracted into a beam structure for damage identification. Next, the influence of damage on the bridge structure was explored from the angles of its inherent frequency and displacement mode, respectively. Our results showed that whether the structure was damaged could be accurately judged by its inherent frequency, but the specific damage could not be further judged. Through the structural displacement curve, the rough range of structural damage could be judged; however, the damage could not be accurately positioned. The damage position could be accurately identified to some extent by taking the derivatives from the difference value of the structural displacement curve. The above conclusions were verified based on a double-span beam. We found that the above conclusions still held true for the double-span beam, thus proving their universality.

Keywords: bridge structure; mode; frequency; displacement curve

Citation: Zhang, Y.; Tan, X.; Li, G.; Dong, J.; Guo, J.; Liu, F. Bridge Structure Damage Identification Based on Dynamic Characteristics. *Coatings* **2022**, *12*, 313. https://doi.org/10.3390/coatings12030313

Academic Editors: Jian Chen, Yanxin Qiao, Fanjiang Meng and Yuxin Wang

Received: 31 December 2021
Accepted: 16 February 2022
Published: 25 February 2022

1. Introduction

Presently, about one-fourth of bridges and buildings in China are affected by hidden structural dangers to a certain degree. It is critical to study the effective means of structural flaw detection to repair these damages. The methods resorting to dynamic characteristics are the current research hotspot. Frequency is the number of times of completing periodical changes within unit time, and the inherent frequency will be reduced owing to the increasing structural damages [1]. Besides, the damages can also be identified by paying attention to the frequency change.

Pandey et al. [2] found that the natural frequency of a bridge is related to the structural mode and shape. Given the structural damage, its stiffness will decline while the structural damping ratio increases.

Hearn and Testa found through a study that after the maximum structural frequency change is normalized, the ratio of changes at any two stages is a damage position function, verified through a model experiment. They further found that a certain law exists between the structural damage and dynamic structural characteristics, but the frequency change is uncorrelated with the evolution of structural damage [3].

Ramanjaneyulu et al. [4] studied the damage identification method based on the structural frequency and vibration mode as well as the effects of changes in different parameters such as frequency, vibration mode, mode curvature and strain energy on the damage identification, positioning and quantification.

Weng built the models of 20–40 m T-beam bridges and box girder bridges via finite element software Midas Civil and explored the relationship between the structural natural vibration frequency and the number of spans of a beam bridge [5].

Hu studied the change in the inherent frequency of a simply supported beam bridge using the fingerprint identification method; established three structural damage fingerprint maps based on the frequency change rate, its quadratic sum and regularized frequency change rate, respectively; conducted a model test; and finally validated the sensitivity of the three fingerprint maps [6].

Wu derived the influences of changes in the structural stiffness and mass on the dynamic characteristics, established a damage identification model based on the mass change according to the variable quantity of inherent structural frequency and verified the feasibility of two methods: additional mass method and a variable quantity of inherent frequency [7–13].

Su conducted the quantitative derivation of structural damage degree based on the displacement curvature and stiffness and proposed different treatment methods for various damages, such as total damage at measuring point and crack damage [14].

Jia constructed a corresponding damage detection system according to the change laws of five parameters related to the damage degree, such as curvature mode value, curvature mode difference and curvature mode ratio [15].

Wei put forward a comprehensive damage identification method based on the inherent frequency and curvature mode and conducted a related study [16].

Lian took the mode curvature as the identification signal, analyzed it using the wavelet transform theory and discovered that the modal curvature difference could overcome the problem of the modal curvature method that fails to identify mild damages [17].

Taking a multiple simply supported beam bridge as the study object, Zhao set the working conditions with one and multiple damages and verified the damage identification accuracy of modal curvature [18–21].

Consequently, the structural damage was simulated in this study mainly by creating directed damages in the structure, mainly studying the change laws of inherent frequency, displacement mode and curvature mode before and after beam structure damage. Furthermore, the nondestructive detection method for structural damage was explored through the change laws of dynamic structural characteristics.

2. Theoretical Derivation

The structural vibration equation could be expressed as a differential equation in the form of an n-order matrix as in Equation (1):

$$M\ddot{u} + C\dot{u} + Ku = f(x) \tag{1}$$

where M is an $n \times n$-order mass stiffness matrix, $\ddot{u}$ denotes an $n \times 1$-order acceleration array, $\dot{u}$ is an $n \times 1$-order velocity array, u stands for an $n \times 1$-order displacement array, K is a stiffness matrix with the $n \times n$-order structure and C is an $n \times n$-order damping matrix.

The damping, which had a minor influence on the structural vibration, could be neglected in terms of the structural natural vibration frequency, so the structure was under a free vibration state. However, $f(x)$ was zero when the structure was not subjected to any external force. Hence, the equation could be rewritten as Equation (2):

$$M\ddot{u} + Ku = 0 \tag{2}$$

Suppose that $u = \varphi e^{j\omega l}$, where φ is the amplitude array of free vibration, and thus the above frequency domain Equation (2) could be written as Equation (3):

$$K\varphi = \omega^2 M\varphi \tag{3}$$

Therefore, the solving of vibration mode and frequency was transformed into the solving of eigenvalue. ω [2] was set as the eigenvalue λ_i and φ_i as the i(th)-order displacement modal vector, so Equation (3) could be expressed alternatively as Equation (4):

$$K\varphi_i = \lambda_i M\varphi_i \tag{4}$$

In case of any damage, the structural stiffness will be changed, and so will its stiffness matrix and the corresponding λ_i and φ_i, as in Equation (5):

$$\delta K_{\varphi i} - \delta\lambda_i M_{\varphi i} = -(K - \lambda_i M)\delta_{\varphi i} \tag{5}$$

where δK, $\delta\lambda_i$ and $\delta_{\varphi i}$ represent the variable quantity of structural stiffness matrix, eigenvalue and eigenvector, respectively. The two sides of Equation (5) are simultaneously multiplied by ω_i^T, and Equation (6) can be acquired by combining Equation (4):

$$\delta\lambda_i = \omega_i^T \delta K \omega_i \tag{6}$$

$\delta K \leq 0$ in the case of any structural damage, so $\delta\lambda_i \leq 0$. $\delta\omega_i \leq 0$ because $\lambda = \omega^2$. Therefore, it could be seen that the structural natural vibration frequency was changed owing to the structural damage. Meanwhile, we found from Equation (6) that when the damage occurred at the same position, the variable quantity of structural natural vibration frequency was enlarged with the increase in the damage degree.

The mode at the corresponding position was changed under the structural damage, while no noticeable change occurred at the position without any damage.

The change of displacement mode before and after the structural damage could be expressed as follows:

$$S = \left|s - s'\right| \tag{7}$$

where s is the displacement mode under the undamaged circumstance and s' represents the displacement mode after the structural damage.

When the structural damage took place, S in Equation (7) increased with the damage degree.

3. Experimental Verification

3.1. Experimental Scheme

This study chose a simply supported beam for the experimental simulation. Polymethyl methacrylate (PMMA) was selected as the structural material at a density of about 1.15–1.19 g/cm [3], conveniently processed and transformed in the laboratory environment. In this experiment, the models selected were simply supported beam (1500 mm × 200 mm × 12 mm) and double-span beam (3200 mm × 200 mm × 12 mm), as shown in Figure 1.

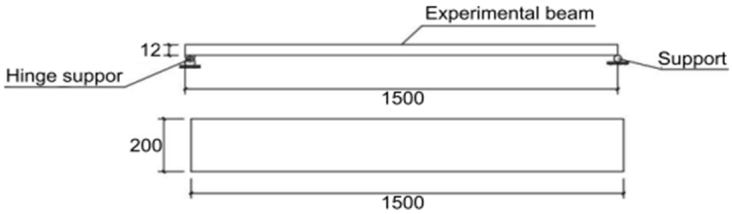

Figure 1. Schematic diagram of experimental beam models.

The working conditions were designed in this experiment using the directed damage assignment method. By reference to many studies, the following three damage conditions were designed (Table 1).

Table 1. Damage conditions.

Condition No.	Span Number	Damage Degree	Damage Position	Number of Damages	Whether Stiffened
Condition 1	Single span	No damage	NO	0	NO
Condition 2	Single span	Single-point 25% damage	1/2 L position	1	NO
Condition 3	Single span	Single-point 25% damage	1/4 L position	1	NO
Condition 4	Single span	Single-point 25% damage	1/2 and 1/4 positions	2	NO

The working conditions are displayed in Figure 2.

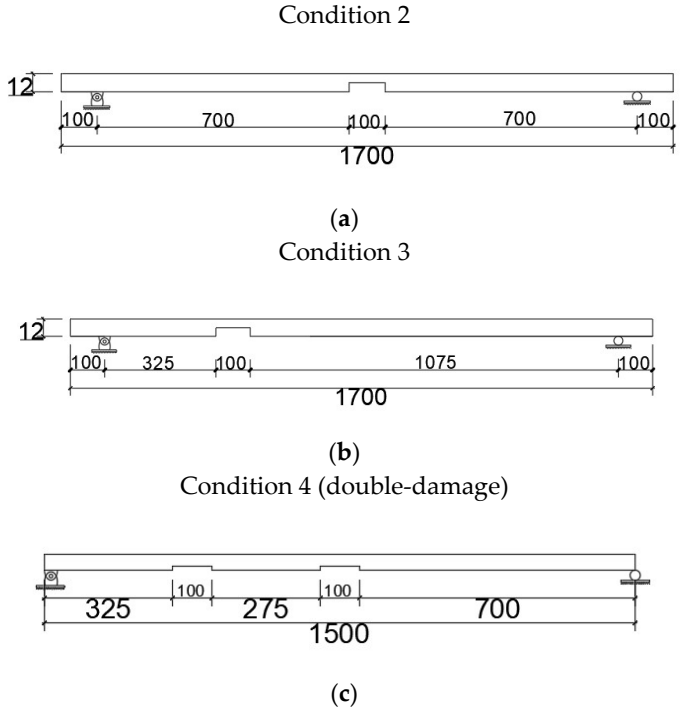

Figure 2. (**a**) Schematic diagram of midspan damage condition; (**b**) schematic diagram of damage condition at 1/4 position; (**c**) schematic diagram of one-span double-damage condition.

To simulate the practical situation in engineering, the models were stiffened. Here, 1400 × 4 × 12 rectangular ribs of the same material were used, and the stiffening forms are as shown in Figure 3.

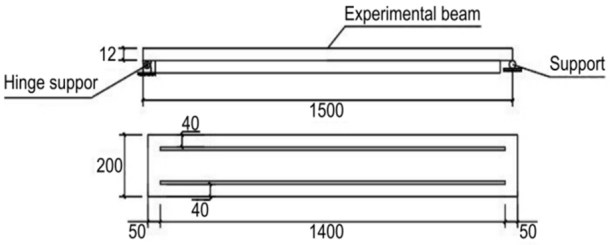

Figure 3. Schematic diagram of models under stiffening conditions.

Therefore, four stiffening conditions were obtained, as listed in Table 2.

Table 2. Summary of stiffened condition.

Condition No.	Span Number	Damage Degree	Damage Position	Number of Damages	Whether Stiffened
Condition 5	Single span	No damage	NO	0	YES
Condition 6	Single span	Single-point 25% damage	1/2 L position	1	YES
Condition 7	Single span	Single-point 25% damage	1/4 L position	1	YES
Condition 8	Single span	Single-point 25% damage	1/2 and 1/4 positions	2	YES

The working conditions are shown in Figure 4.

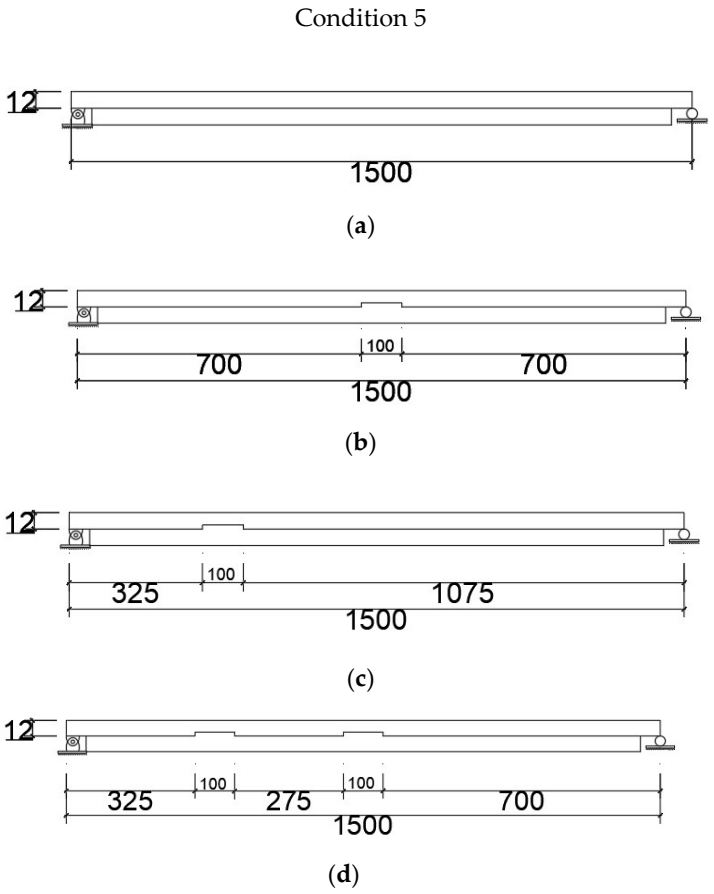

Figure 4. (**a**) Schematic diagram of stiffened and nondamaged condition; (**b**) schematic diagram of stiffened and midspan damage condition; (**c**) schematic diagram of stiffened and damage condition (1/4 position); (**d**) schematic diagram of stiffened and one-span double-damage condition.

The sensor system used in the experiment was composed of INV3018CT 24-bit high-precision data acquisition instrument (Figure 5), computer, force hammer, sensor, double-sided adhesive tape, test piece and two-way crystal interface cable.

The layout of experimental measuring points and excitation points is displayed below. The experimental beam was divided into 15 equal parts, the sensor was fixed at points 5 and 7 (Figure 6), the excitation points were numbered 1–16, the excitation was conducted at each excitation point three times and the average of three results was taken.

(**a**) (**b**) (**c**)

Figure 5. INV3018CT 24-bit high-precision data acquisition instrument, force hammer and sensor. (**a**) Instrument host; (**b**) Stress hammer; (**c**) Sensor.

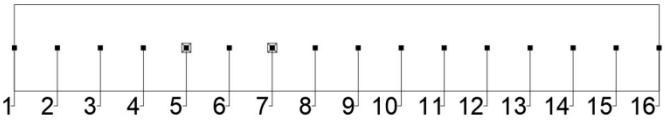

Figure 6. Layout plan of measuring points.

Coinv Dasp V11 software matching with the experimental instrument was used for the data processing. The model graph and animated graph of vibration mode could be automatically generated in the software, as shown in Figures 7 and 8.

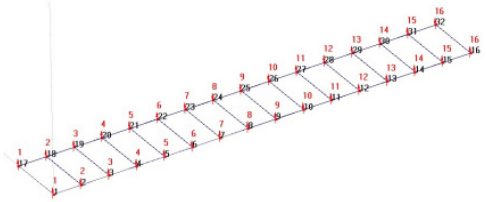

Figure 7. Automatically generated model graph.

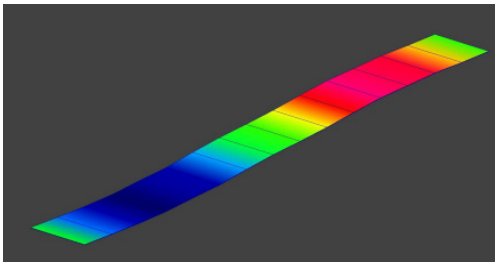

Figure 8. Animated graph of vibration mode.

3.2. Experimental Data and Analysis

3.2.1. Damage Identification Analysis Based on the Inherent Frequency

As one of the dynamic structural characteristics, the inherent frequency can reflect the structural damage condition to some extent. Therefore, the inherent frequencies under different damage conditions obtained through the experiment were compared with those under undamaged conditions. Next, the loss rate of inherent frequency under each vibration mode was calculated by taking the nondamaged and stiffened condition and nondamaged and unstiffened condition (Condition 5 and Condition 1) as the criteria. The comparison results are listed in Tables 3 and 4.

Table 3. Frequency loss rates under different damage conditions.

Order of Vibration Mode	Condition 1	Condition 2		Condition 3		Condition 4	
	Frequency (Hz)	Frequency (Hz)	Frequency Loss Rate %	Frequency (Hz)	Frequency Loss Rate %	Frequency (Hz)	Frequency Loss Rate %
1	6.4435	6.376	1.05	6.325	1.84	6.212	3.59
2	19.043	18.176	4.55	18.837	1.08	18.031	5.31
3	40.746	39.826	2.26	39.328	3.48	39.548	2.94
4	69.659	68.301	1.95	68.841	1.17	68.965	1.00
5	111.789	110.365	1.27	111.425	0.33	110.348	1.29

Table 4. Frequency loss rates under different stiffening conditions.

Order of Vibration Mode	Condition 5	Condition 6		Condition 7		Condition 8	
	Frequency (Hz)	Frequency (Hz)	Frequency Loss Rate %	Frequency (Hz)	Frequency Loss Rate %	Frequency (Hz)	Frequency Loss Rate %
1	13.948	13.917	0.22	13.833	0.82	13.803	1.04
2	48.057	46.684	2.86	47.751	0.64	48.363	3.52
3	103.68	102.13	1.49	103.30	0.37	103.29	4.23
4	170.74	167.56	1.86	167.44	1.93	164.45	3.68
5	216.65	215.76	0.41	216.36	0.13	215.78	1.79

The above tables show that the inherent structural frequency was reduced due to the damage. By comparing the frequency loss rates under Conditions 2 and 3 with those under Conditions 6 and 7, it could be known that the structural frequency was significantly more changed by the midspan damage than by the damage at the 1/4 position. Meanwhile, the frequencies of the second- and third-order vibration modes were changed significantly, while the gap of the first order with the fourth and fifth orders became smaller and smaller. Based on the above results, it could be obtained that the frequency loss brought by the current damage condition was smaller and smaller with the order change of vibration mode. By comparing the structural frequency loss rates under Conditions 1–4 with those under Conditions 5–6, it could be seen that the stiffness of stiffened structure was enhanced, so the frequency loss caused by the structural damage was reduced relative to that before the stiffening.

3.2.2. Damage Identification Based on Displacement Mode

According to the previous section, we found that the inherent frequency only reflected whether the structure was damaged but failed to determine the damage position, so the structural displacement mode was exported in this section for the study. Like the frequency study part, two groups were formed: stiffened and nonstiffened groups, and the undamaged conditions within the two groups were compared. The displacement mode under Condition 1 (single-span nondamaged) was compared with that under Condition 2 (midspan damage), as shown in Figure 9.

The comparison graphs of displacement modes under Condition 1 (single-span nondamaged) and Condition 3 (damage at the 1/4 position), as shown in Figure 10.

The comparison results of displacement modes at different orders under Condition 1 (single-span nondamaged) and Condition 4 (single-span double-damage) are shown in Figure 11.

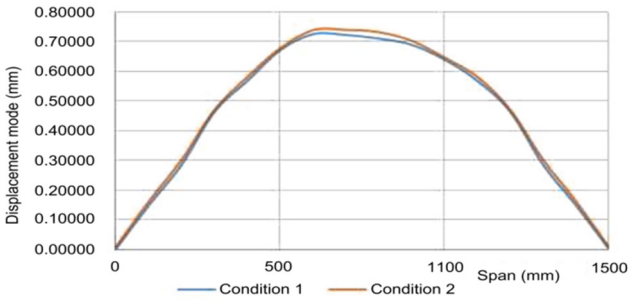

(**a**) Comparison of the first-order vibration modes under Conditions 1 and 2.

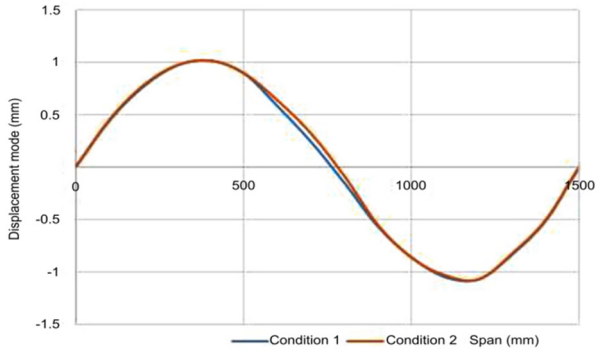

(**b**) Comparison of the second-order vibration modes under Conditions 1 and 2.

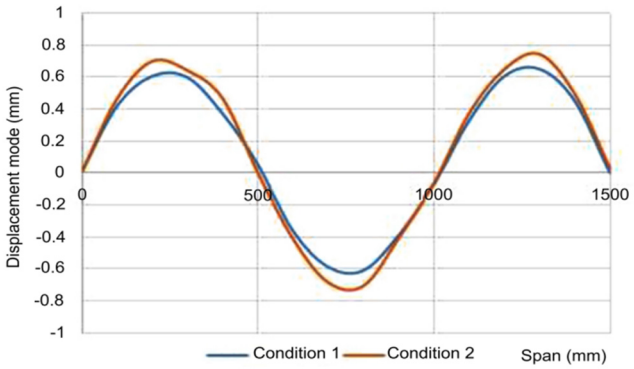

(**c**) Comparison of the third-order vibration modes under Conditions 1 and 2.

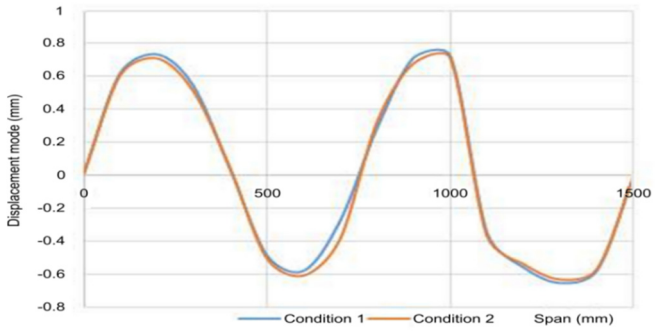

(**d**) Comparison of the fourth-order vibration modes under Conditions 1 and 2.

Figure 9. *Cont.*

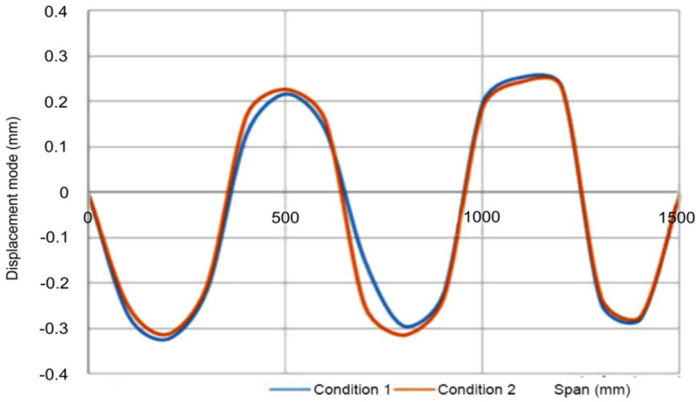

(**e**) Comparison of the fifth-order vibration modes under Conditions 1 and 2.

Figure 9. Comparison of first five orders of vibration modes under Conditions 1 and 2.

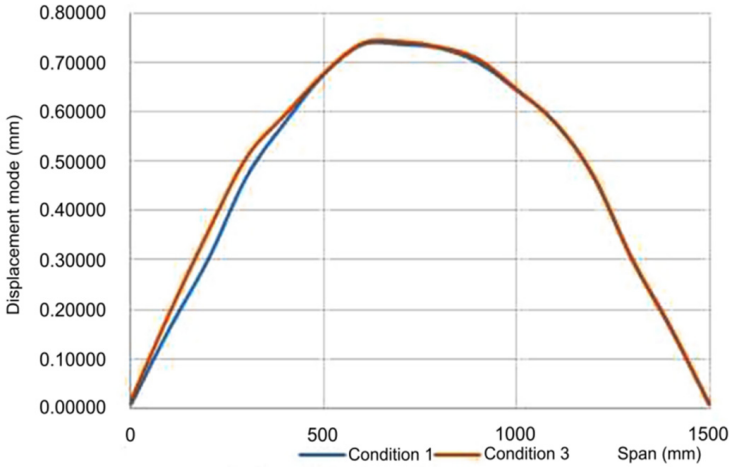

(**a**) Comparison of the first-order vibration modes under Conditions 1 and 3.

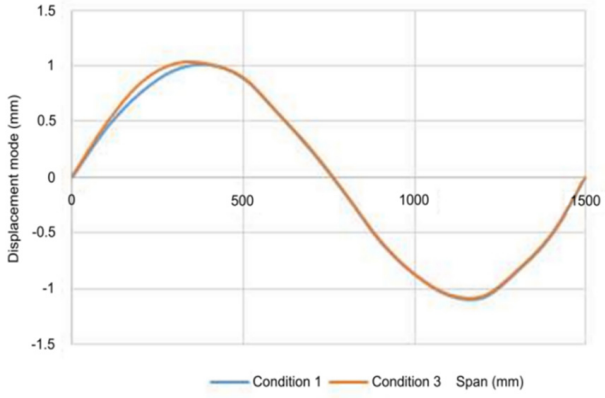

(**b**) Comparison of the second-order vibration modes under Conditions 1 and 3.

Figure 10. *Cont.*

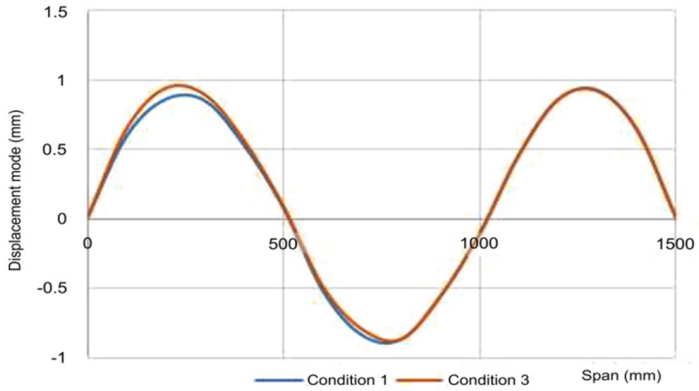

(**c**) Comparison of the third-order vibration modes under Conditions 1 and 3.

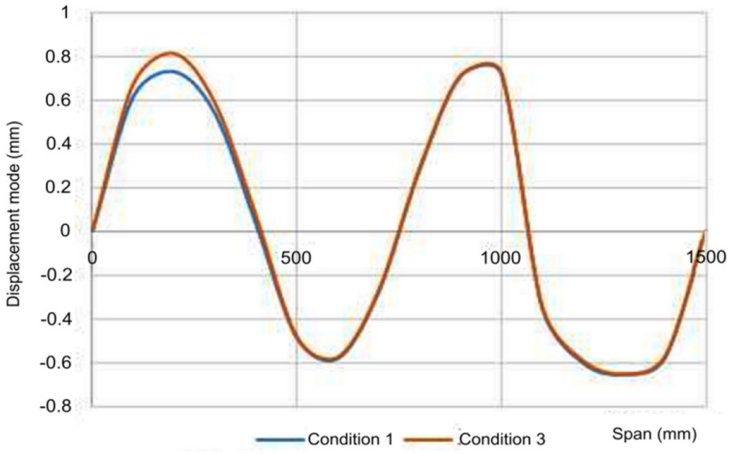

(**d**) Comparison of the fourth-order vibration modes under Conditions 1 and 3.

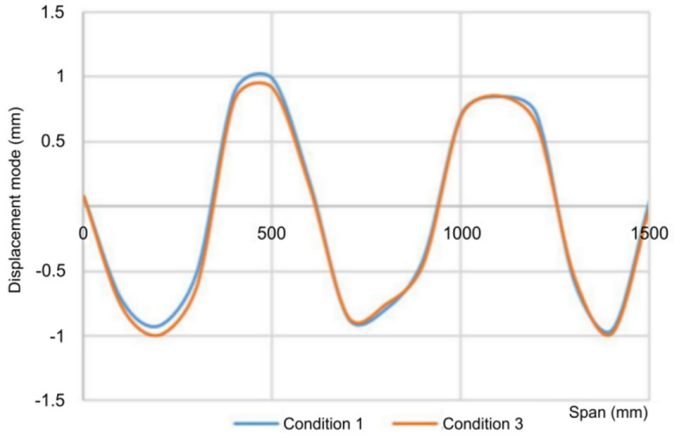

(**e**) Comparison of the fifth-order vibration modes under Conditions 1 and 3.

Figure 10. Comparison of the first five orders of vibration modes under Conditions 1 and 3.

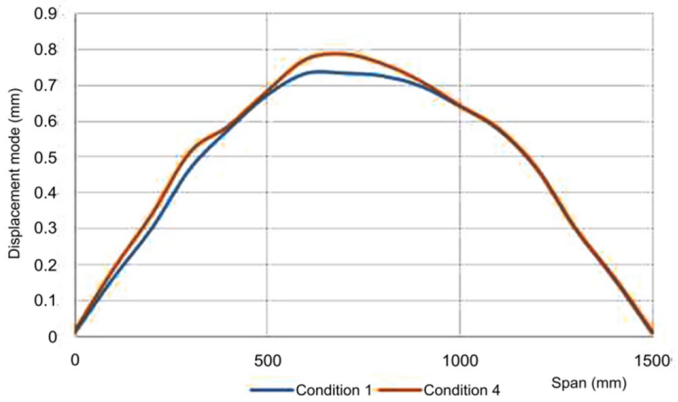

(**a**) Comparison of the first-order vibration modes under Conditions 1 and 4.

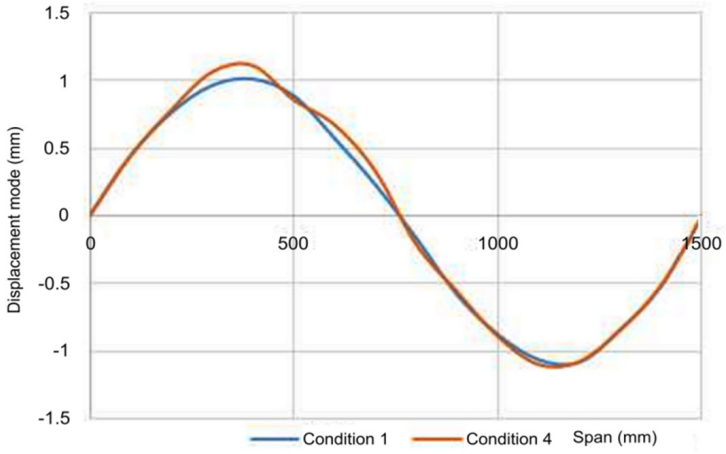

(**b**) Comparison of the second-order vibration modes under Conditions 1 and 4.

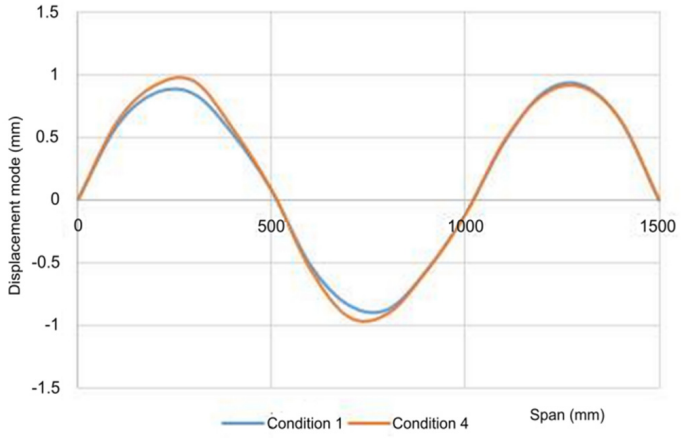

(**c**) Comparison of the third-order vibration modes under Conditions 1 and 4.

Figure 11. *Cont.*

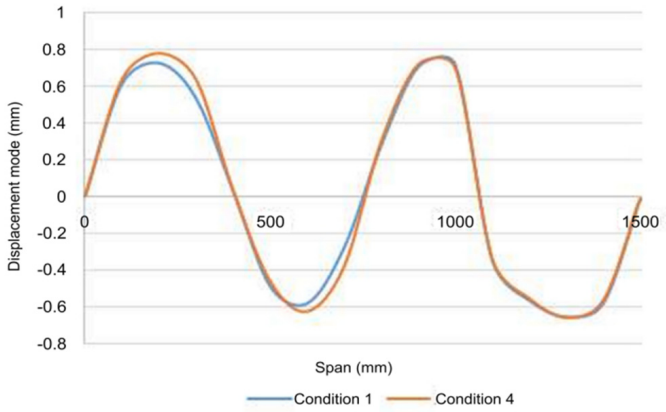

(**d**) Comparison of the fourth-order vibration modes under Conditions 1 and 4.

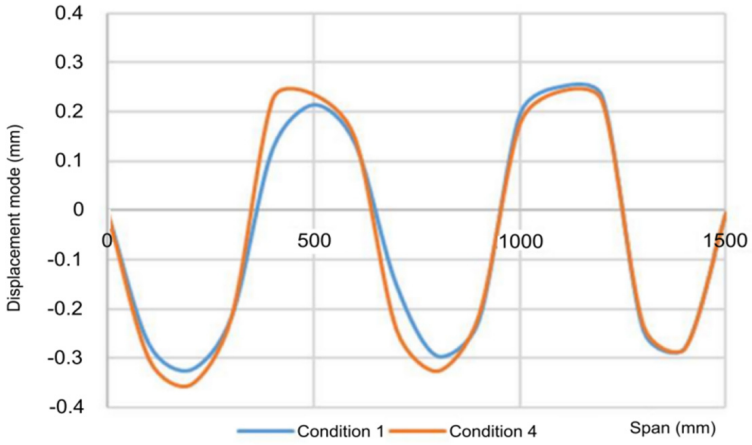

(**e**) Comparison of the fifth-order vibration modes under Conditions 1 and 4.

Figure 11. Comparison of the first five orders of vibration modes under Conditions 1 and 4.

The comparison results of displacement modes under Condition 5 (stiffened and nondamaged) and Condition 6 (stiffened and midspan damage) are shown in Figure 12.

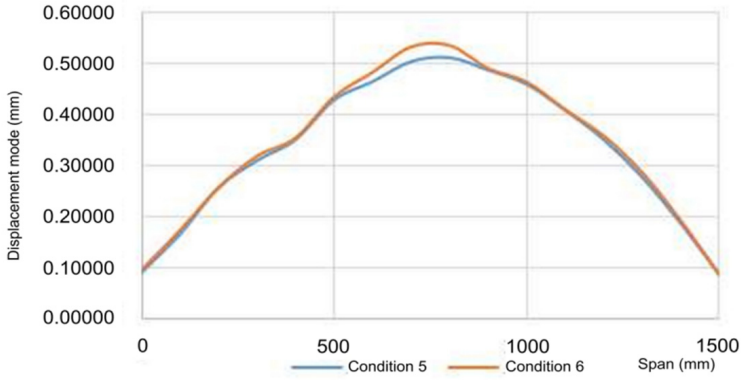

(**a**) Comparison of the first-order vibration modes under Conditions 5 and 6.

Figure 12. *Cont.*

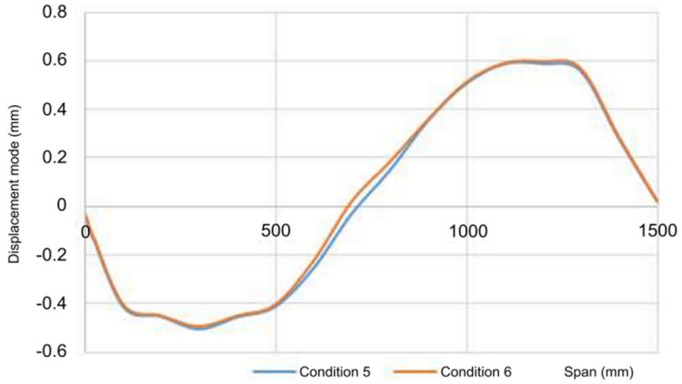

(**b**) Comparison of the second-order vibration modes under Conditions 5 and 6.

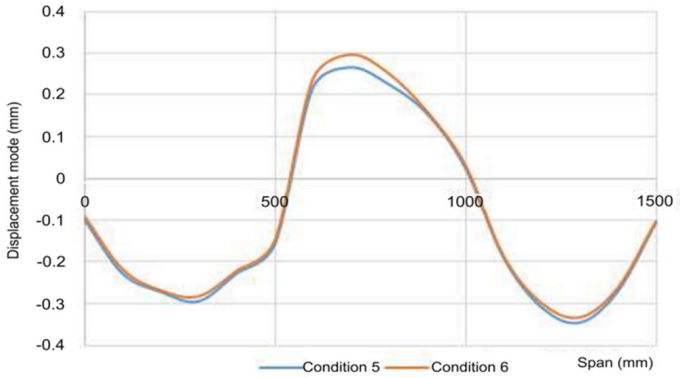

(**c**) Comparison of the third-order vibration modes under Conditions 5 and 6.

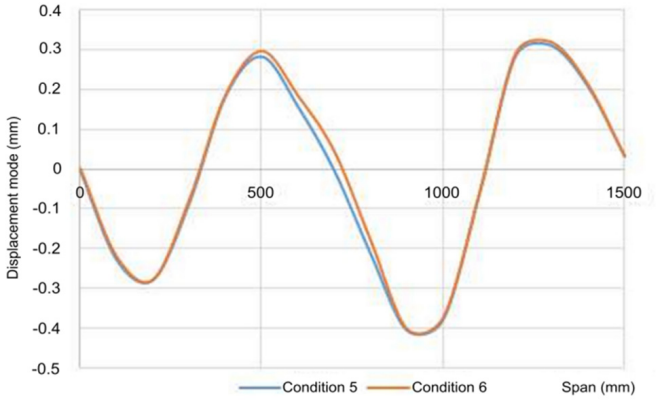

(**d**) Comparison of the fourth-order vibration modes under Conditions 5 and 6.

Figure 12. *Cont.*

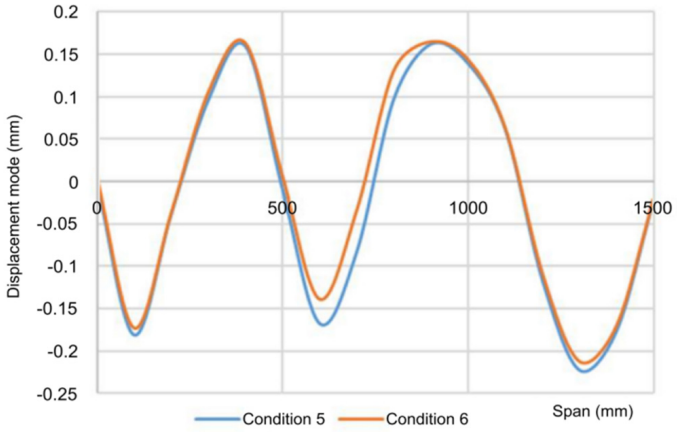

(**e**) Comparison of the fifth-order vibration modes under Conditions 5 and 6.

Figure 12. Comparison of the first five orders of vibration modes under Conditions 5 and 6.

The displacement modes under Condition 5 (stiffened and nondamaged) and Condition 7 (stiffened and damaged at the 1/4 position) were compared, as shown in Figure 13.

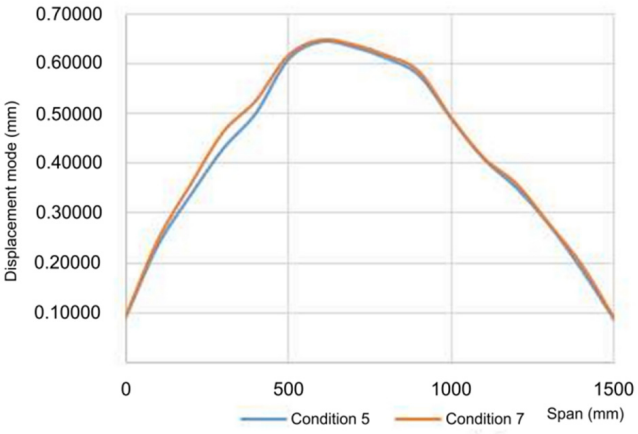

(**a**) Comparison of the first-order vibration modes under Conditions 5 and 7.

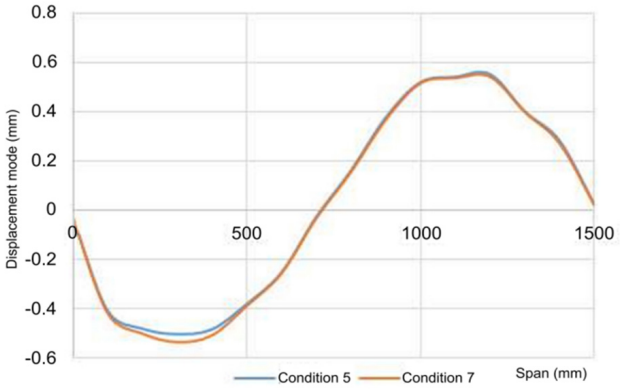

(**b**) Comparison of the second-order vibration modes under Conditions 5 and 7.

Figure 13. *Cont.*

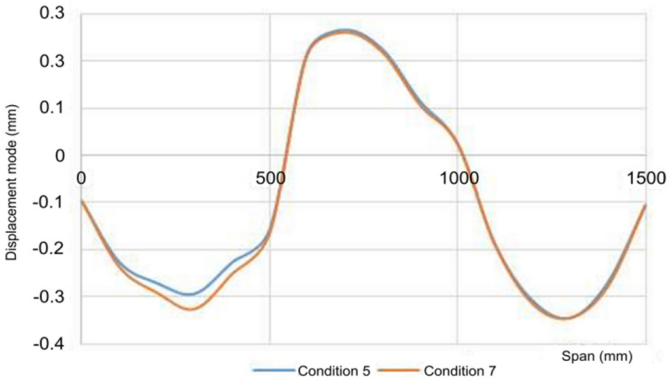

(**c**) Comparison of the third-order vibration modes under Conditions 5 and 7.

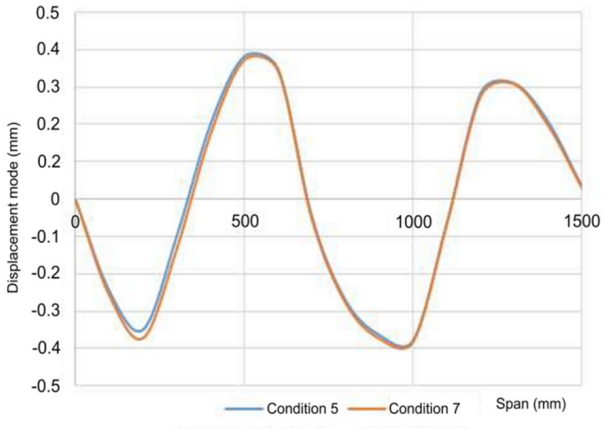

(**d**) Comparison of the fourth-order vibration modes under Conditions 5 and 7.

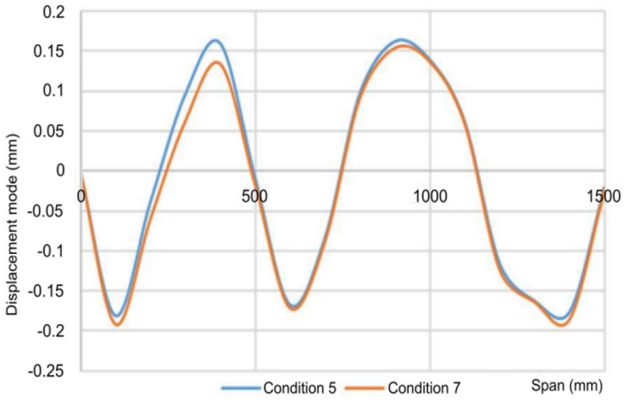

(**e**) Comparison of the fifth-order vibration modes under Conditions 5 and 7.

Figure 13. Comparison of the first five orders of vibration modes under Conditions 5 and 7.

The comparison results of displacement modes under Condition 5 (stiffened and nondamaged) and Condition 8 (stiffened and double-damage) are shown in Figure 14.

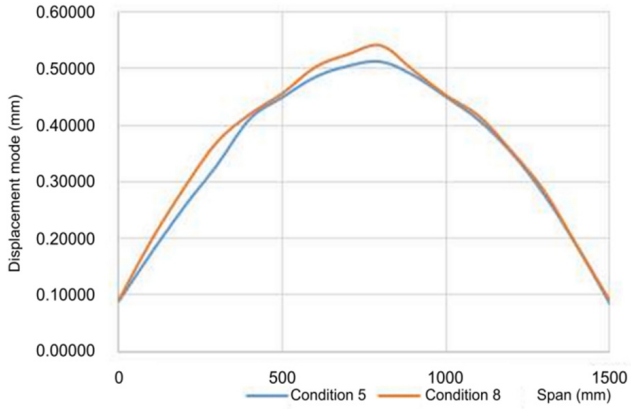

(**a**) Comparison of the first-order vibration modes under Conditions 5 and 8.

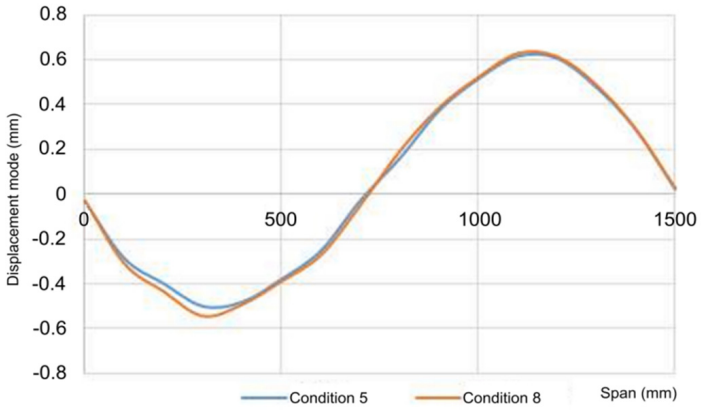

(**b**) Comparison of the second-order vibration modes under Conditions 5 and 8.

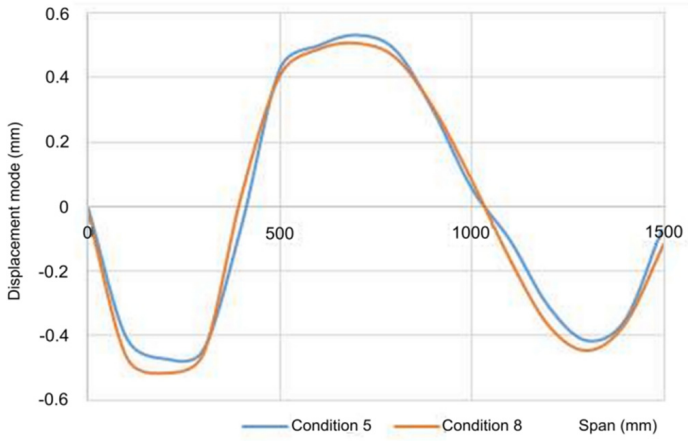

(**c**) Comparison of the third-order vibration modes under Conditions 5 and 8.

Figure 14. *Cont.*

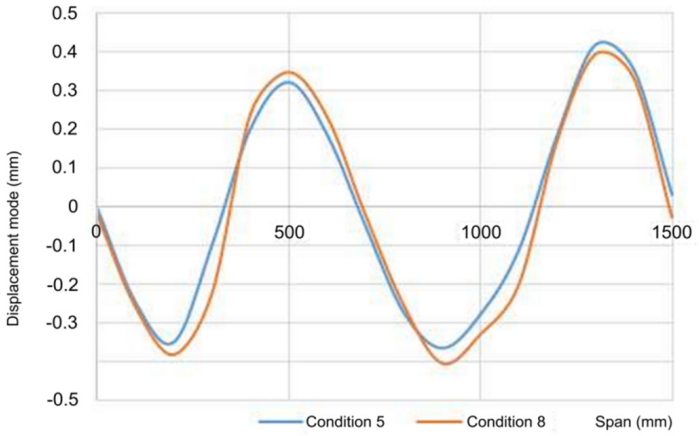

(**d**) Comparison of the fourth-order vibration modes under Conditions 5 and 8.

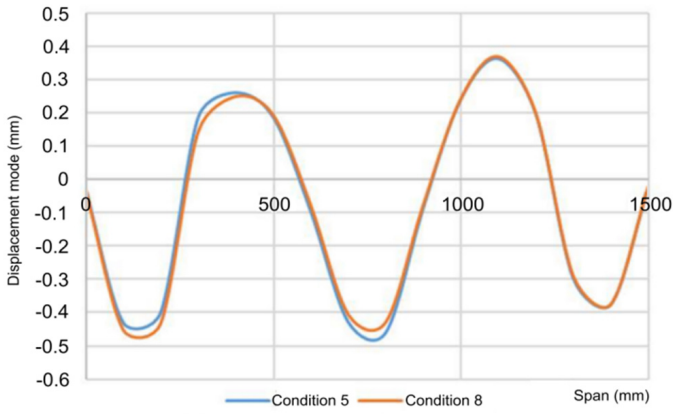

(**e**) Comparison of the fifth-order vibration modes under Conditions 5 and 8.

Figure 14. Comparison of the first five orders of vibration modes under Conditions 5 and 8.

The displacement modes obtained through the experiment under the damaged and undamaged conditions were compared in the same coordinate system. It appeared that the displacement amplitude at the damage position under the damage condition was different from that at the same position under the nondamaged condition, and the displacement amplitude difference under the stiffening condition was smaller than that under the nonstiffened condition. To conveniently view the specific damage position, the displacement mode curve was amplified by taking the derivatives of difference value, which could obtain the first-order and second-order derivatives of displacement mode difference, as shown from Figures 9–14.

By comparing the graphs in Figure 15, the first-order and second-order derivatives of the first-order vibration mode difference fluctuated significantly at two middle points, which conformed to the directed additional working condition in the experiment. However, the difference derivatives of the second- to fifth-order vibration modes did not show any significant fluctuation point, and the position of given damage could not be observed through the curve. Hence, it was concluded that the first-order vibration mode had better sensitivity to the damage during the damage identification. Therefore, the derivatives were continuously taken from the difference between Conditions 1 and 3 and that between Conditions 1 and 4, and the first-order and second-order derivatives of the first-order vibration mode were further obtained, as shown in Figures 16 and 17, respectively.

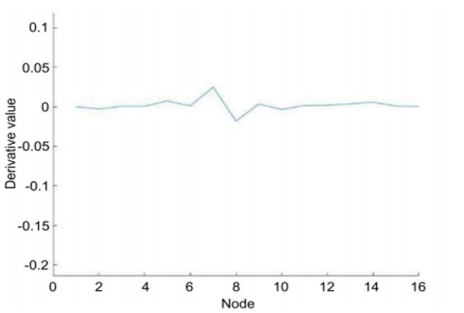

(**a**) First-order derivative of first-order mode difference.

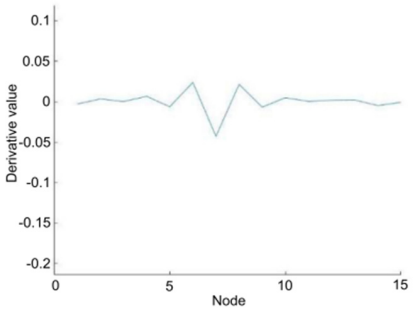

(**b**) Second-order derivative of first-order mode difference.

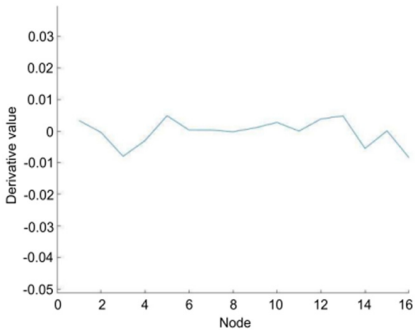

(**c**) First-order derivative of second-order mode difference.

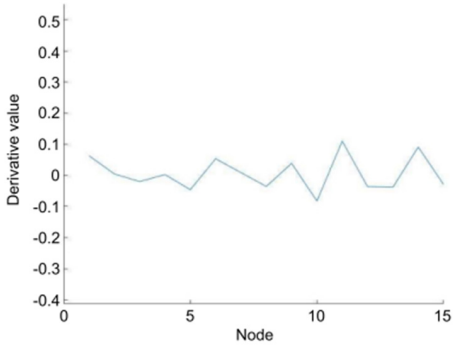

(**d**) Second-order derivative of second-order mode difference.

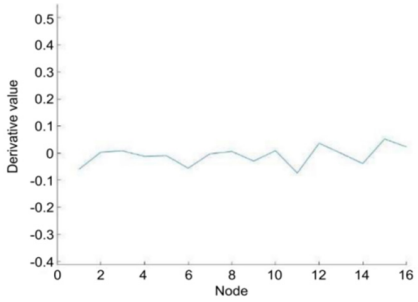

(**e**) First-order derivative of third-order mode difference.

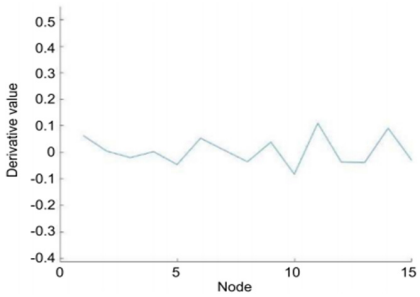

(**f**) Second-order derivative of third-order mode difference.

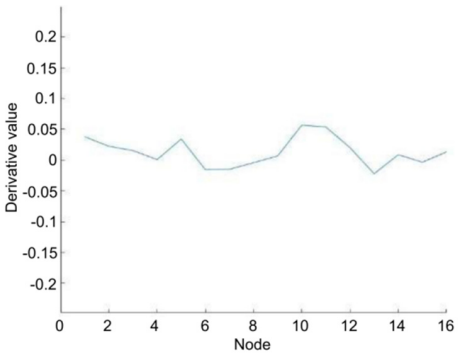

(**g**) First-order derivative of fourth-order mode difference.

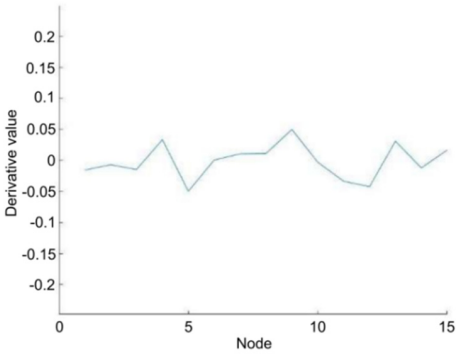

(**h**) Second-order derivative of fourth-order mode difference.

Figure 15. *Cont.*

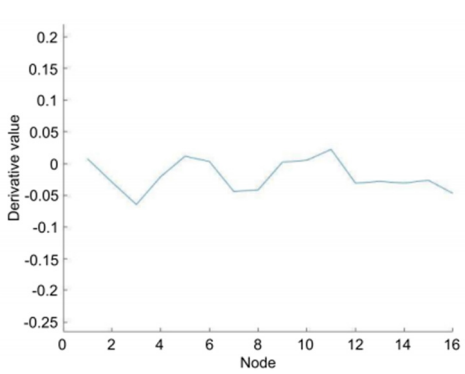

(**i**) First-order derivative of fifth-order mode difference.

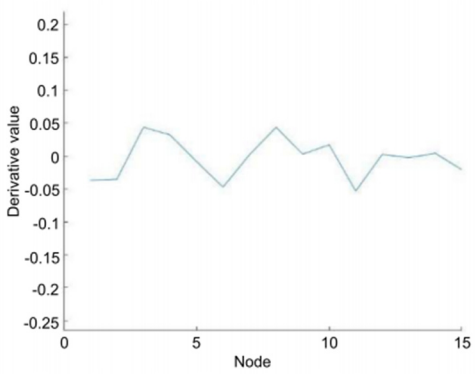

(**j**) Second-order derivative of fifth-order mode difference.

Figure 15. First-order and second-order derivative curves of the differences of the first five orders of modes under Conditions 1 and 2.

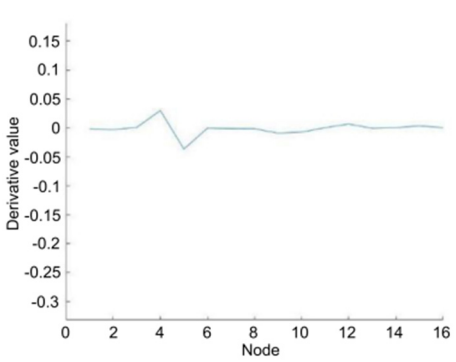

(**a**) First-order derivative of first-order mode difference.

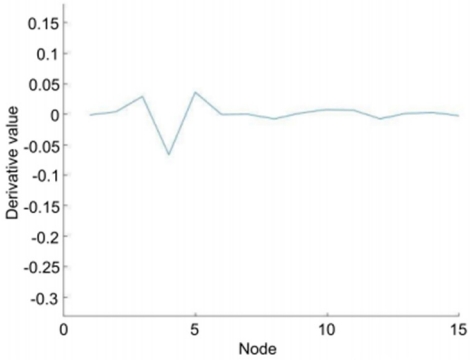

(**b**) Second-order derivative of first-order mode difference.

Figure 16. Difference derivatives under Conditions 1 (single-span and nondamaged) and 3 (damage at the 1/4 position).

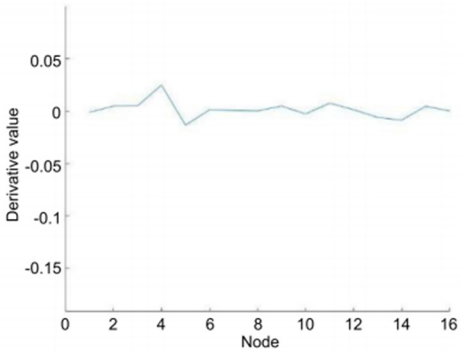

(**a**) First-order derivative of first-order mode difference.

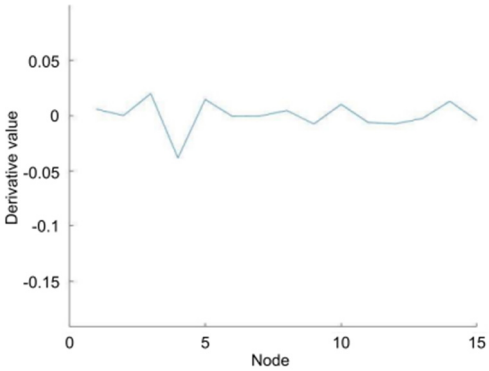

(**b**) Second-order derivative of first-order mode difference.

Figure 17. Difference derivatives under the Conditions 1 (single-span nondamaged) and 4 (single-span double-damage).

Under the single-span double-damage condition, we found that the first-order derivative of the first-order mode difference fluctuated at the damage position. The fluctuations in the other graphs were noticeable but uniform, and the damage position could not be observed. By continuously solving the first-order derivatives of first-order mode difference

under the stiffening condition, the above conclusion was still verified to be true, and the first-order derivative curves of first-order mode difference under the stiffening condition are displayed in Figures 18–20.

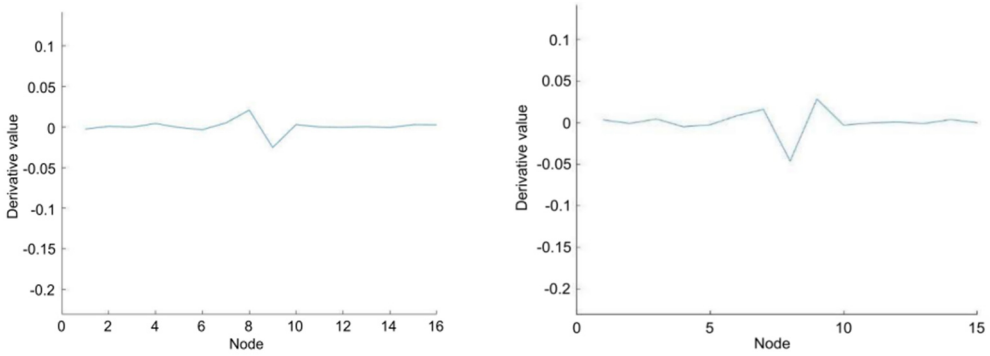

(**a**) First-order derivative of first-order mode difference.

(**b**) Second-order derivative of first-order mode difference.

Figure 18. First-order and second-order derivative curves of the differences of the first five orders of modes under Conditions 5 and 6.

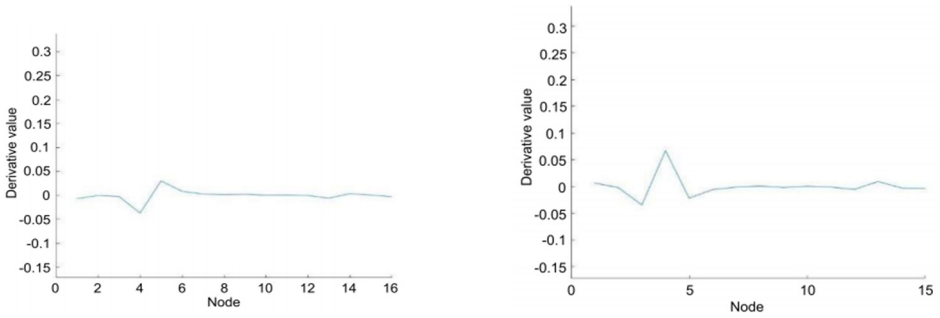

(**a**) First-order derivative of first-order mode difference.

(**b**) Second-order derivative of first-order mode difference.

Figure 19. First-order and second-order derivative curves of the differences of the first five orders of modes under Conditions 5 and 7.

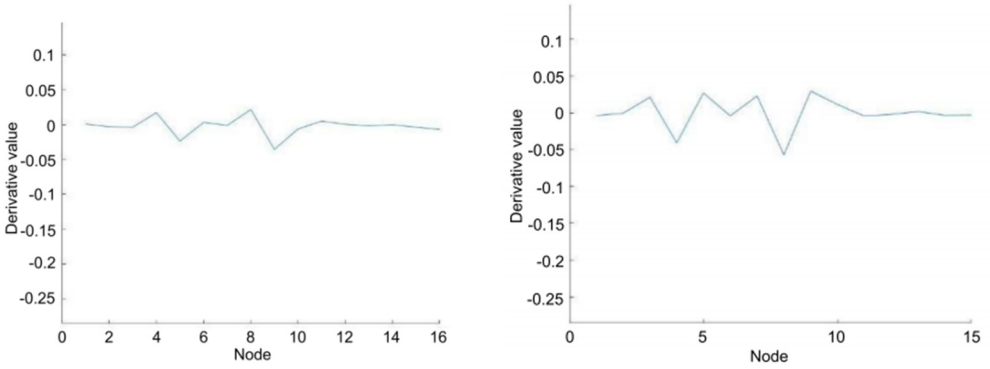

(**a**) First-order derivative of first-order mode difference.

(**b**) Second-order derivative of first-order mode difference.

Figure 20. First-order and second-order derivatives of the differences of the first five orders of modes under Conditions 5 and 8.

Similarly, the conclusion consistent with the previous section could be obtained by comparing the first-order and second-order derivative curves of vibration mode differences at different orders: the first-order derivative of first-order vibration mode difference experienced a major fluctuation in the case of structural damage, but the other curves showed no evident trends.

3.3. Finite Element Simulation

3.3.1. Simulation Effect Analysis of Inherent Frequency

The finite element method is a numerical method used to solve the numerical solution to the set of differential equation sets or integral equation sets. In this experiment, the modeling was conducted using ABAQUS, and the modeling effect graphs are shown in Figures 21 and 22.

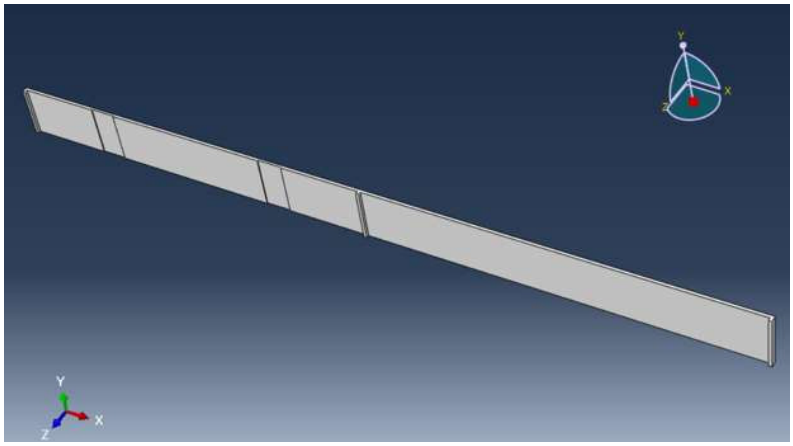

Figure 21. Model graph after the creation of damage and support.

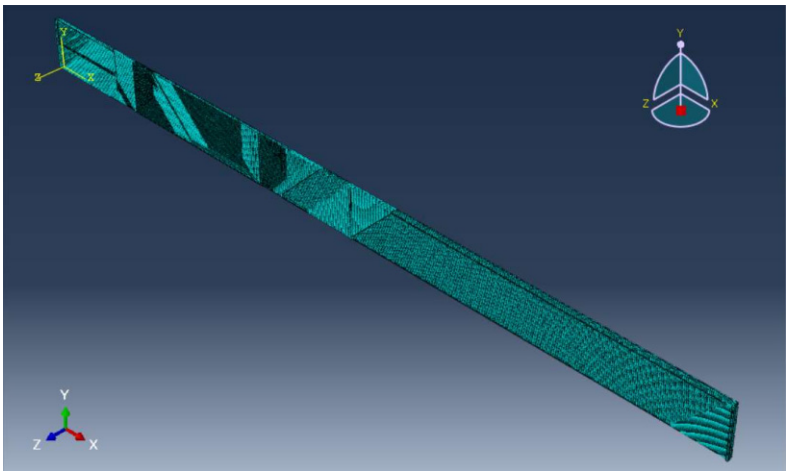

Figure 22. Model graph after the mesh generation.

Under ideal conditions, the inherent structural frequency could be obtained by establishing a finite element model. The theoretical value and experimentally measured value of inherent frequency were compared, as listed in Table 5.

Table 5. Inherent frequency errors.

Order of Vibration Mode	Condition 1			Condition 2		
	Measured Frequency (Hz)	Simulated Frequency (Hz)	Percentage Error %	Measured Frequency (Hz)	Simulated Frequency (Hz)	Percentage Error %
1	6.4435	7.3394	−12.21	6.376	7.2711	−12.31
2	19.043	20.597	−7.54	18.176	20.555	−11.57
3	40.746	41.022	−0.67	39.826	39.912	−0.22
4	69.659	68.751	1.32	68.301	68.302	0.00
5	111.789	103.84	7.66	110.365	102.434	7.74
Order of Vibration Mode	**Condition 3**			**Condition 4**		
	Measured Frequency (Hz)	Simulated Frequency (Hz)	Percentage Error %	Measured Frequency (Hz)	Simulated Frequency (Hz)	Percentage Error %
1	6.325	7.3327	−13.74	6.212	7.1989	−13.71
2	18.837	20.43	−7.80	18.031	20.134	−10.45
3	39.328	39.714	−0.97	39.548	38.858	1.78
4	68.841	68.242	0.88	68.965	68.366	0.88
5	111.425	101.8	9.45	110.348	101.34	8.89
Order of Vibration Mode	**Condition 5**			**Condition 6**		
	Measured Frequency (Hz)	Simulated Frequency (Hz)	Percentage Error %	Measured Frequency (Hz)	Simulated Frequency (Hz)	Percentage Error %
1	6.325	7.3327	−13.74	6.212	7.1989	−13.71
2	18.837	20.43	−7.80	18.031	20.134	−10.45
3	39.328	39.714	−0.97	39.548	38.858	1.78
4	68.841	68.242	0.88	68.965	68.366	0.88
5	111.425	101.8	9.45	110.348	101.34	8.89
Order of Vibration Mode	**Condition 7**			**Condition 8**		
	Measured Frequency (Hz)	Simulated Frequency (Hz)	Percentage Error %	Measured Frequency (Hz)	Simulated Frequency (Hz)	Percentage Error %
1	6.325	7.3327	−13.74	6.212	7.1989	−13.71
2	18.837	20.43	−7.80	18.031	20.134	−10.45
3	39.328	39.714	−0.97	39.548	38.858	1.78
4	68.841	68.242	0.88	68.965	68.366	0.88
5	111.425	101.8	9.45	110.348	101.34	8.89

We found that the experimentally measured result was not much different from the simulated result in the numerical value; the two presented the consistent change laws, they deviated a lot from each other only at the fifth order and both percentage errors did not exceed 15%. This revealed that the construction method of the finite element model was correct and accorded with reality. The inherent frequency loss rates of the vibration modes at different orders under the simulated conditions are listed in Table 6.

As seen in Table 6, the frequency loss rates of the second- and third-order vibration modes were the maximum. It could be observed that the inherent frequency of each order under the stiffening conditions (Conditions 5 to 8) was always greater than that under the nonstiffened conditions (Conditions 1 to 4). Meanwhile, the frequency loss rate brought by the midspan damage was higher than triggered by the damage at the 1/4 position. Both abovementioned laws indicated the variation trends of experimental data, manifesting that the experimental data are approximate to the simulated data and the frequencies of both the second-order and third-order vibration modes can be taken as the criteria for the damage identification.

Table 6. Inherent frequency loss rates at different orders.

Order of Vibration Mode	Condition 1	Condition 2		Condition 3		Condition 4	
	Frequency (Hz)	Frequency (Hz)	Frequency Loss Rate %	Frequency (Hz)	Frequency Loss Rate %	Frequency (Hz)	Frequency Loss Rate %
1	7.3394	7.2711	0.93	7.3327	0.09	7.1989	1.91
2	20.597	20.555	0.20	20.43	0.81	20.134	2.25
3	41.022	39.912	2.71	39.714	3.19	38.858	5.28
4	68.751	68.302	0.65	68.242	0.74	68.366	0.56
5	103.84	102.434	1.35	101.8	1.96	101.34	2.41
Order of Vibration Mode	**Condition 5**	**Condition 6**		**Condition 7**		**Condition 8**	
	Frequency (Hz)	Frequency (Hz)	Frequency Loss Rate %	Frequency (Hz)	Frequency Loss Rate %	Frequency (Hz)	Frequency Loss Rate %
1	13.948	13.717	1.66	13.833	0.82	13.903	0.32
2	48.057	48.684	−1.30	47.751	0.64	48.363	−0.64
3	103.68	102.13	1.49	103.30	0.37	103.29	0.38
4	170.74	167.56	1.86	167.44	1.93	164.45	3.68
5	216.65	215.76	0.41	216.36	0.13	215.78	0.40

3.3.2. Simulation Curve Analysis of Displacement Mode

The mode curves at different orders under Conditions 1 to 4 and those under Conditions 5 to 8 were plotted into the same graphs, as shown in Figures 23 and 24, respectively.

It can be observed from Figure 6-1 that although each curve deviated from the nondamaged condition due to the damage, this was consistent with the experimentally measured result, indicating that it is feasible to take the derivatives from the displacement mode difference. To eliminate the disturbance triggered by the experimental errors and further verify the sensitivity of the first-order derivative of structural first-order mode difference to the damage, the derivatives were also taken from the simulated displacement mode difference under the vibration mode at each order, and whether the variation trends were identical with the experimental results was checked. The derivative curves of vibration mode differences at different orders under the simulated Condition 1 (single-span nondamaged) and Condition 2 (midspan damage) are shown in Figure 25.

By comparing the above curves that after the number of points was expanded, the obvious numerical fluctuations could be manifested by the first-order vibration mode; moreover, the damage scope could be primarily defined by the first-order or third-order derivatives of vibration mode at each order, too. However, the first-order derivative of the first-order vibration mode was still relatively more apparent. The derivative curves of vibration mode differences at different orders under the simulated Conditions 1 (single-span nondamaged) and 3 (damage at the 1/4 position), as shown in Figure 26.

Figure 26 shows that the damage could be positioned by all the first-order derivative graphs of difference values. Besides, the damage position could also be reflected by some second-order derivatives. In the curves, the fluctuation amplitude of first-order derivatives for the first-order vibration mode differences was the minimum. Although the curve of the nondamaged part presented continuous oscillation, it could be regarded as an approximately straight line, so the first-order derivative curves of first-order vibration modes still had the superiority compared to the other curves. The derivative curves of displacement mode differences at different orders under Condition 5 (single-span nondamaged) and Condition 8 (one-span double-damage) are shown in Figure 27.

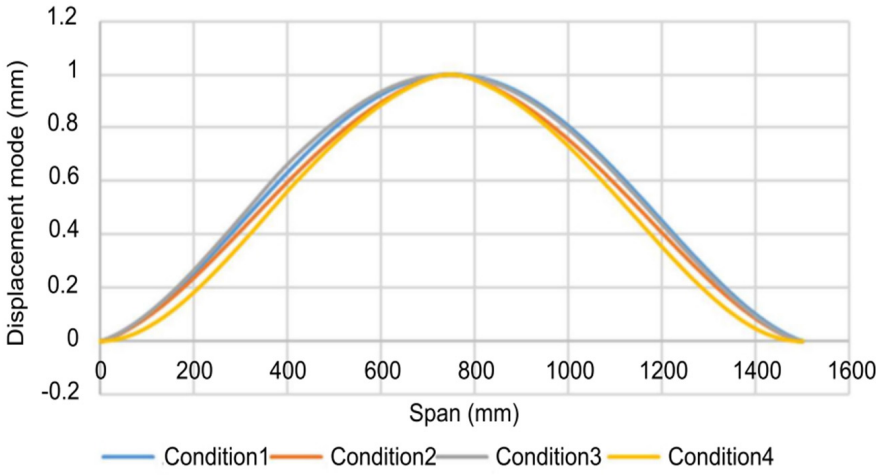

(**a**) First order vibration mode.

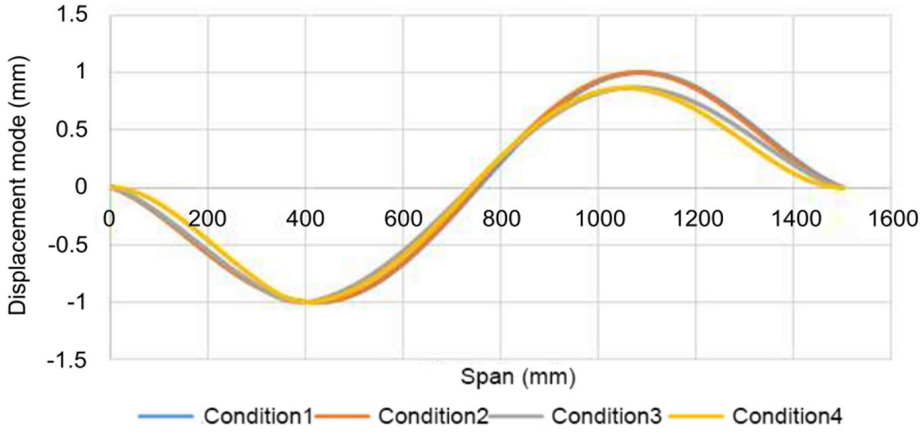

(**b**) Second order vibration mode.

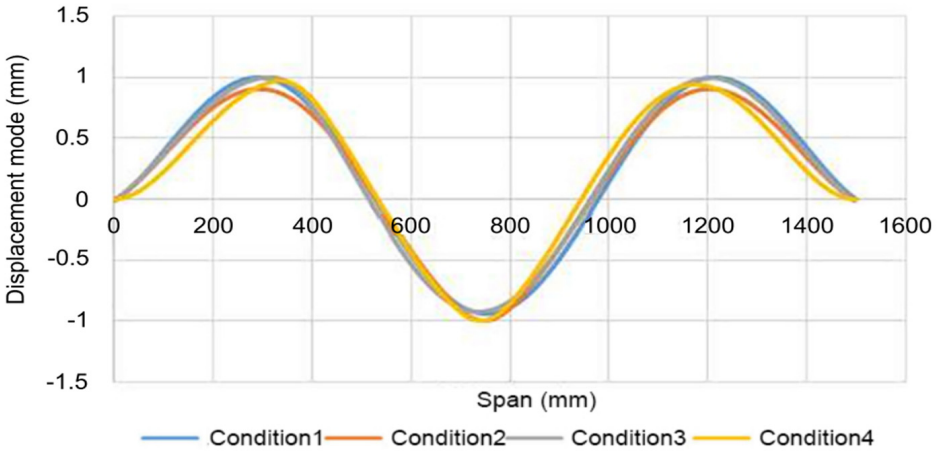

(**c**) Third order vibration mode.

Figure 23. *Cont.*

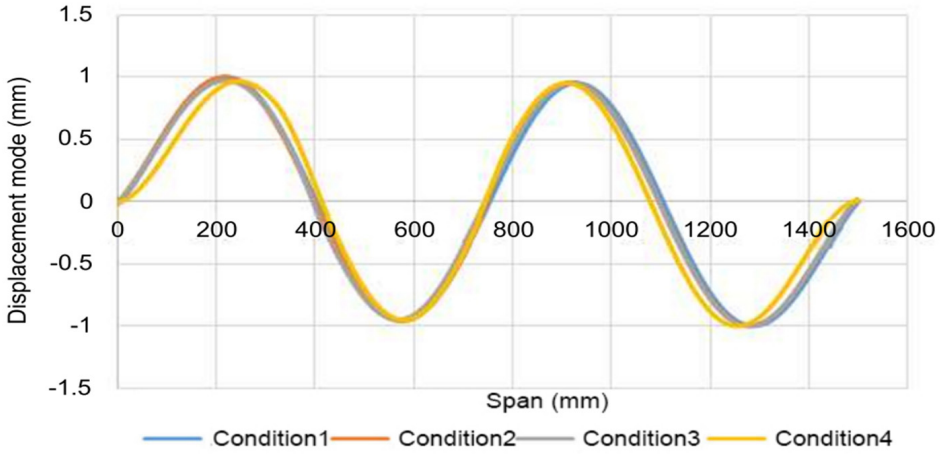

(**d**) Fouth order vibration mode.

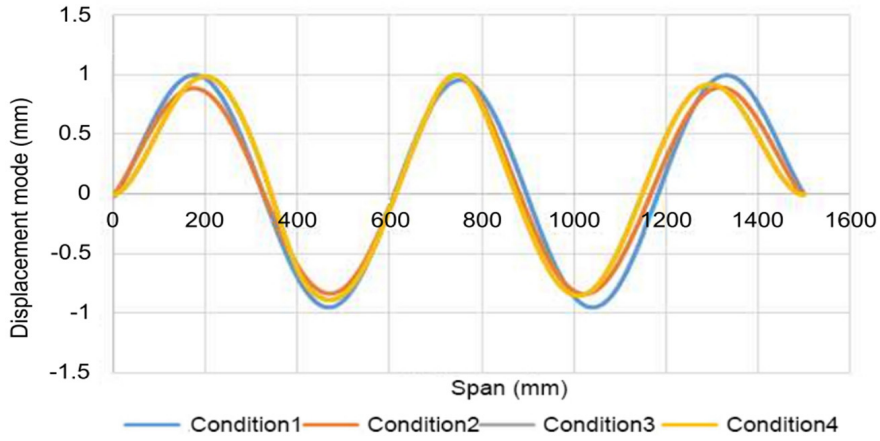

(**e**) 5th order vibration mode.

Figure 23. Comparison of mode curves at different orders under Conditions 1 to 4.

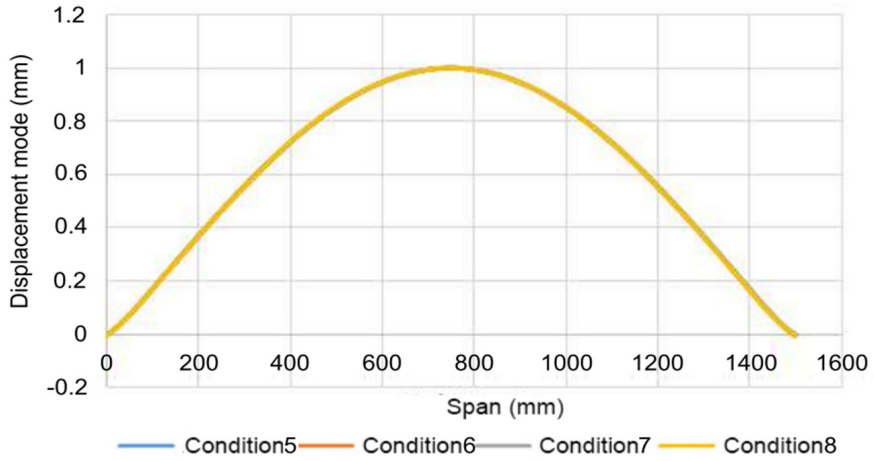

(**a**) First order vibration mode.

Figure 24. *Cont.*

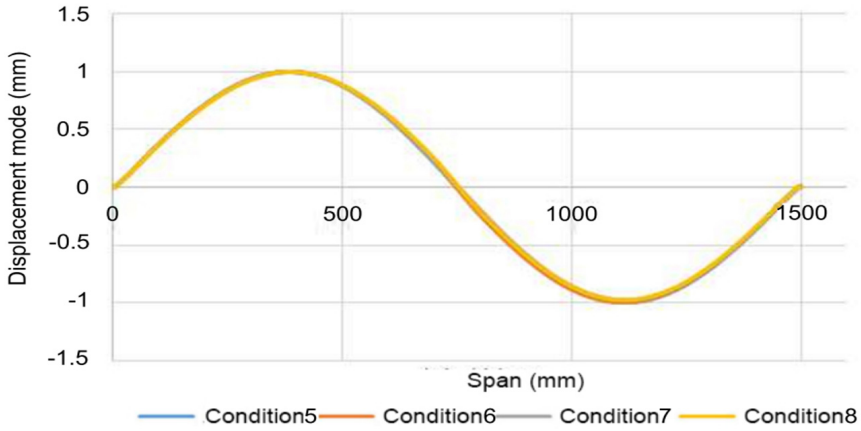

(**b**) Second order vibration mode.

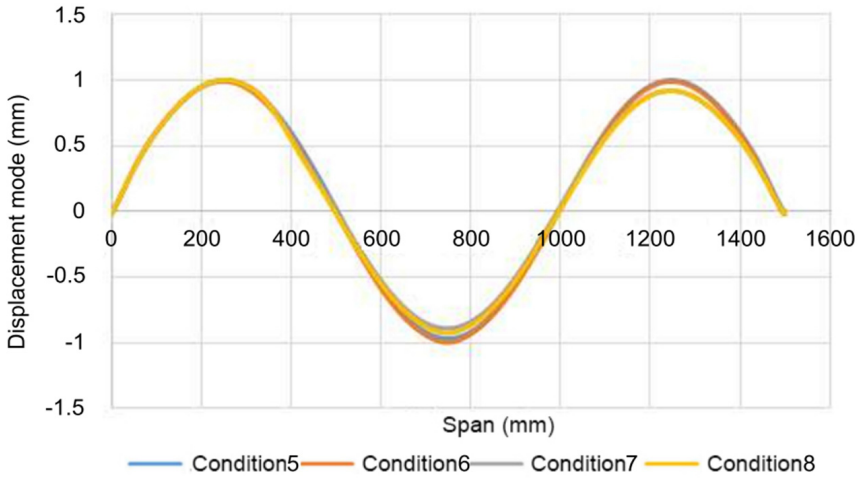

(**c**) Third order vibration mode.

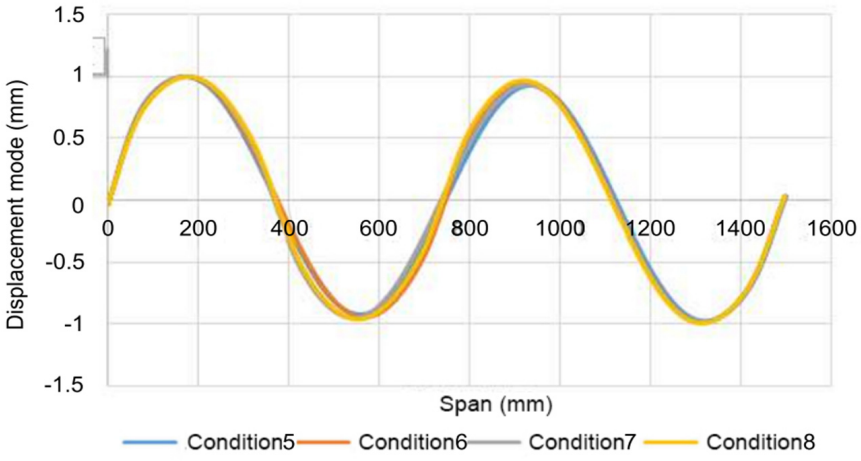

(**d**) Fouth order vibration mode.

Figure 24. *Cont.*

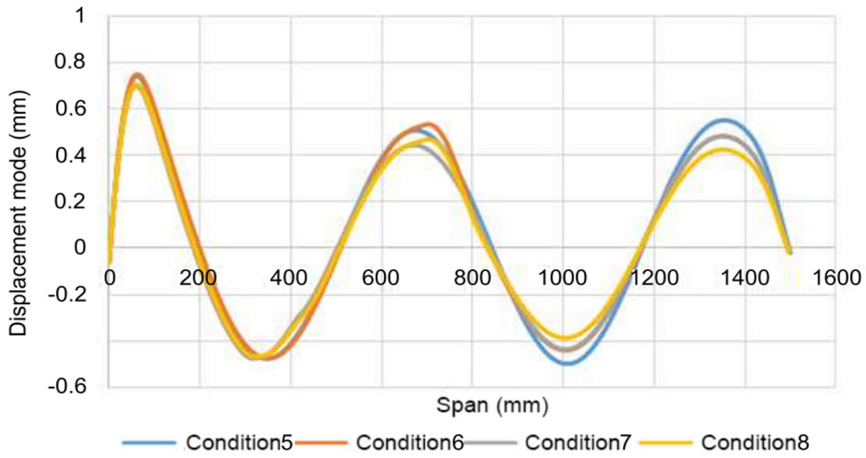

(**e**) 5th order vibration mode.

Figure 24. Displacement mode curves at different orders under Conditions 5 to 8.

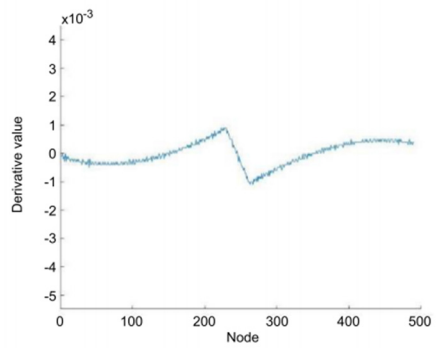

(**a**) First-order derivative of first-order mode difference.

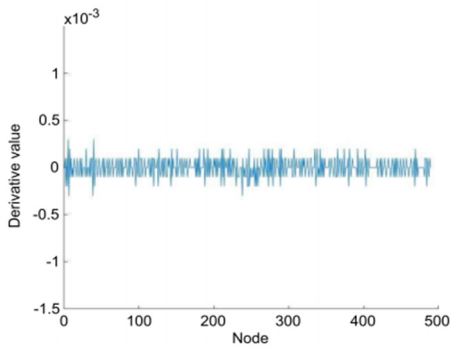

(**b**) Second-order derivative of second-order mode difference.

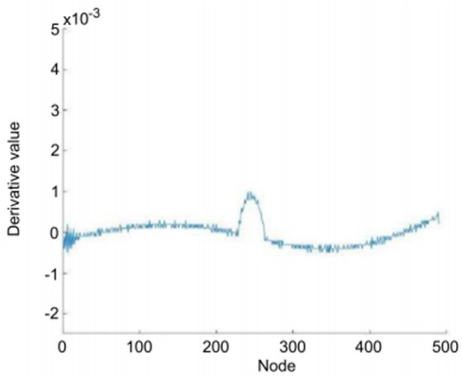

(**c**) First-order derivative of second-order mode difference.

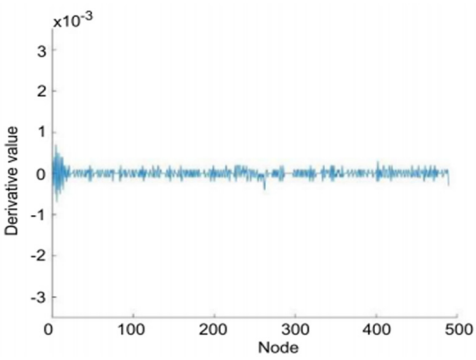

(**d**) Second-order derivative of second-order mode difference.

Figure 25. *Cont.*

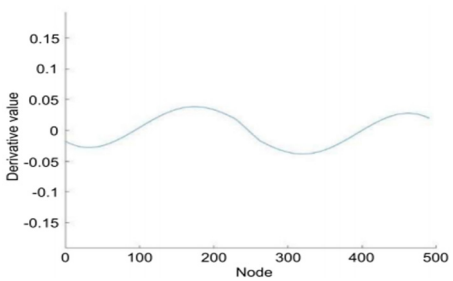

(**e**) First-order derivative of third-order mode difference.

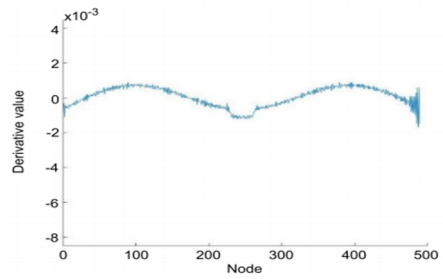

(**f**) Second-order derivative of third-order mode difference.

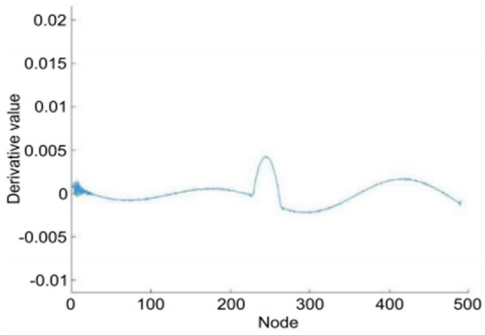

(**g**) First-order derivative of fourth-order mode difference.

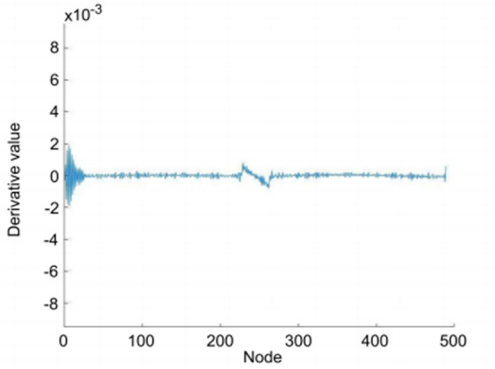

(**h**) Second-order derivative of fourth-order mode difference.

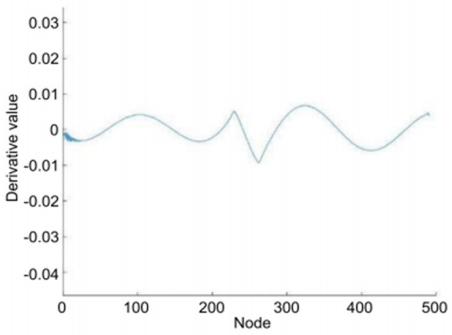

(**i**) First-order derivative of fifth-order mode difference.

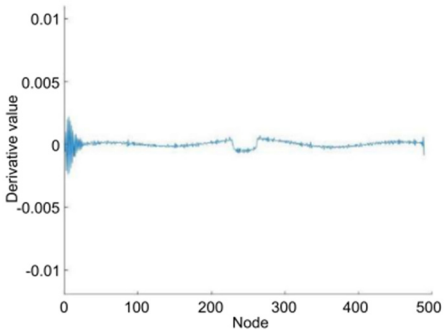

(**j**) Second-order derivative of fifth-order mode difference.

Figure 25. First-order and second-order derivatives of the differences of the first five orders of modes under Conditions 1 and 4.

Restricted by the length of the paper, the other conditions are not described in detail. The damage position could be reflected through the data simulation by both the first-order derivative curves of each vibration mode difference and most second-order derivative curves. Similarly, the first-order derivative of first-order vibration mode difference owned a smoother curve in the undamaged part, which embodied the superiority of first-order derivative curves of first-order vibration mode difference over the other first-order derivative curves.

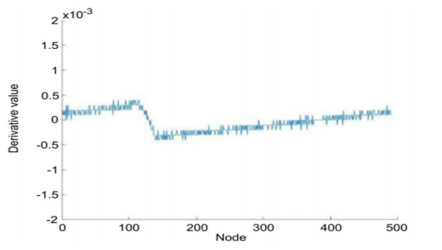

(**a**) First-order derivative of first-order mode difference.

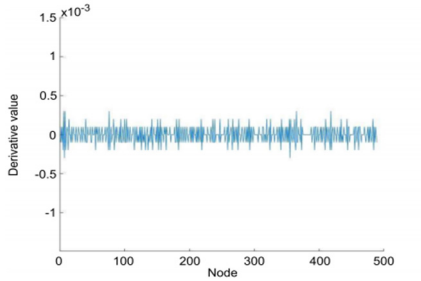

(**b**) Second-order derivative of first-order mode difference.

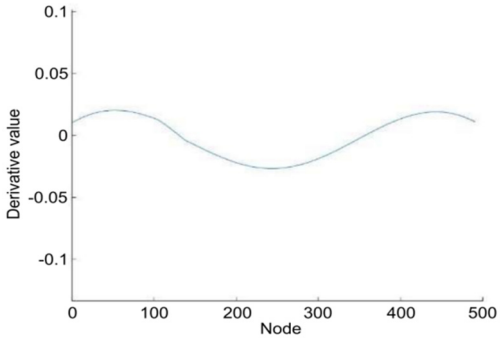

(**c**) First-order derivative of second-order mode difference.

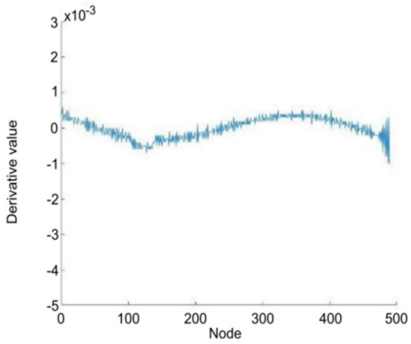

(**d**) Second-order derivative of second-order mode difference.

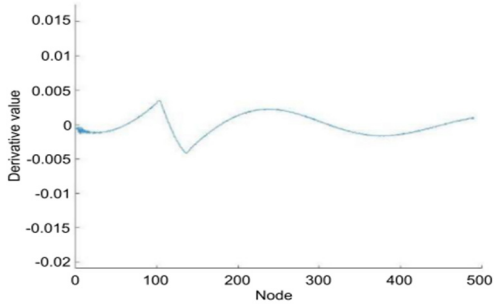

(**e**) First-order derivative of third-order mode difference

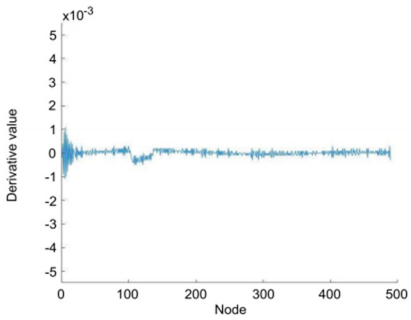

(**f**) Second-order derivative of third-order mode difference.

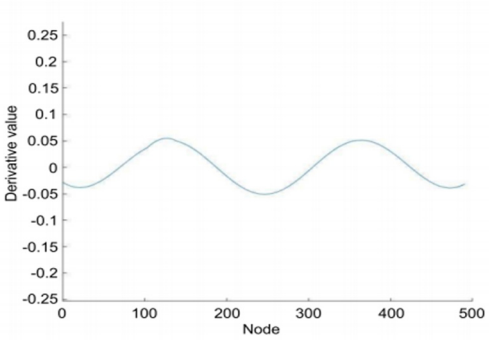

(**g**) First-order derivative of fourth-order mode difference

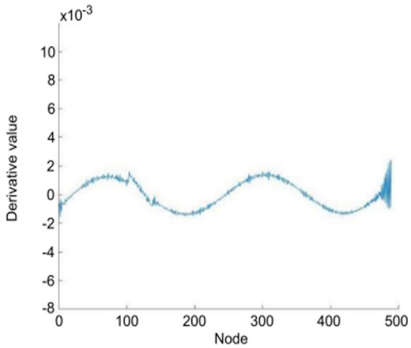

(**h**) Second-order derivative of fourth-order mode difference.

Figure 26. *Cont.*

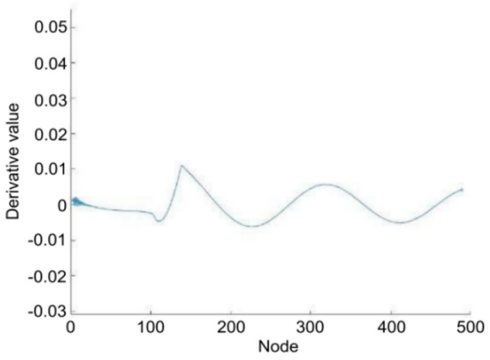

(**i**) First-order derivative of fifth-order mode difference

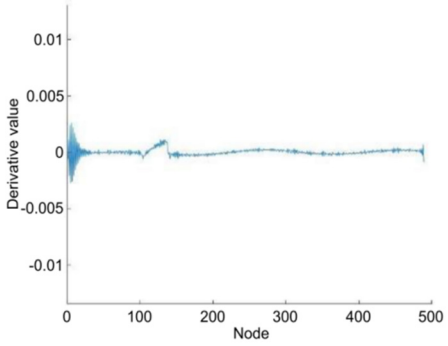

(**j**) Second-order derivative of fifth-order mode difference.

Figure 26. First-order and second-order derivatives of the differences of the first five orders of modes under Conditions 1 and 3.

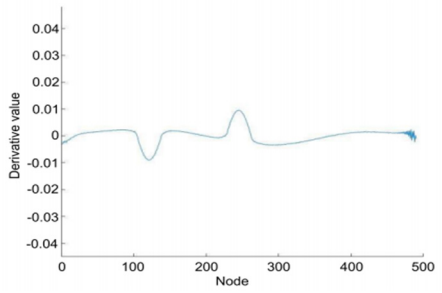

(**a**) First-order derivative of first-order mode difference.

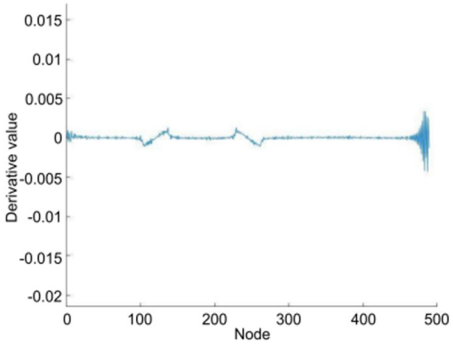

(**b**) Second-order derivative of first-order mode difference.

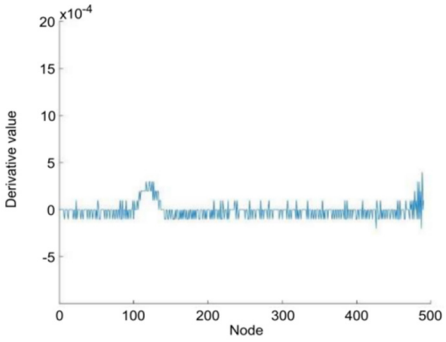

(**c**) First-order derivative of second-order mode difference.

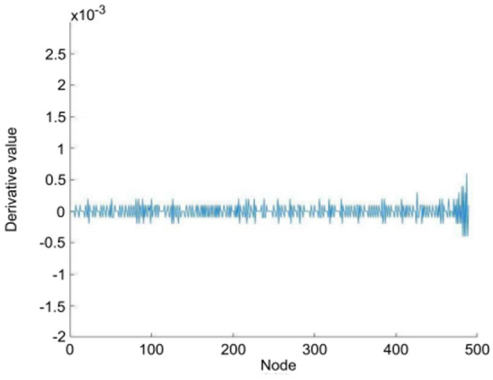

(**d**) Second-order derivative of second-order mode difference.

Figure 27. *Cont.*

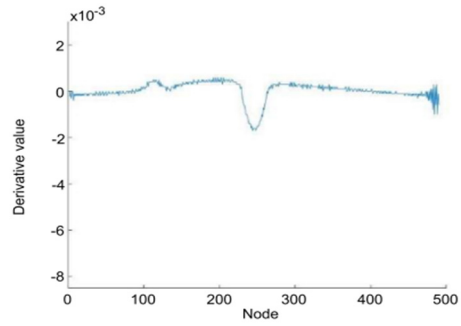

(**e**) First-order derivative of third-order mode difference.

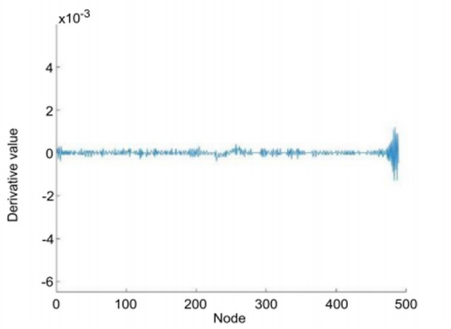

(**f**) Second-order derivative of third-order mode difference.

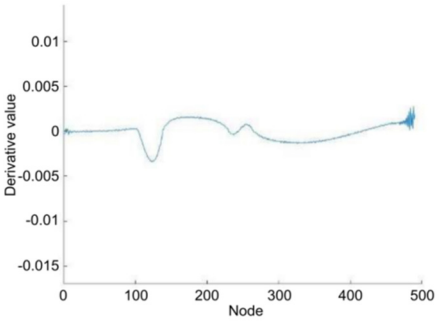

(**g**) First-order derivative of fourth-order mode difference.

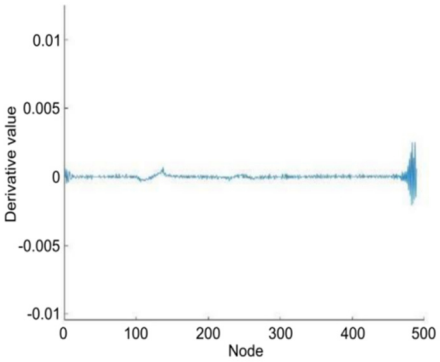

(**h**) Second-order derivative of fourth-order mode difference.

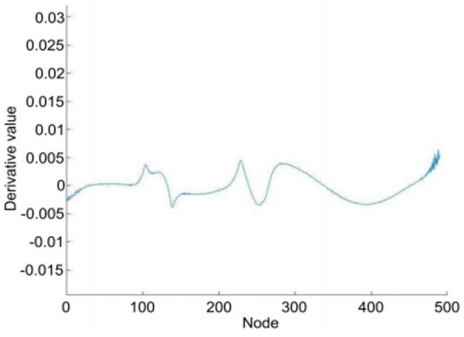

(**i**) First-order derivative of fifth-order mode difference.

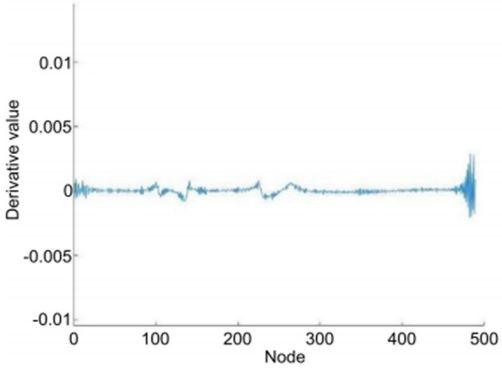

(**j**) Second-order derivative of fifth-order mode difference.

Figure 27. First-order and second-order derivatives of the differences of the first five orders of modes under Conditions 5 and 8.

3.4. Validation by Case Simulation

A double-span continuous beam was designed and different damage conditions were set to validate whether the conclusions above applied to the other structural forms. The case model is displayed in Figure 28, and the working conditions of this case are listed in Table 7.

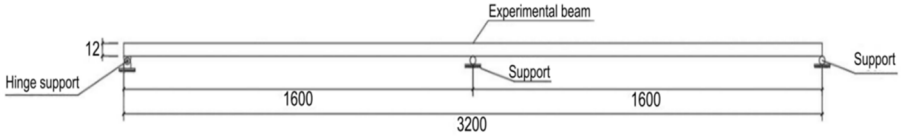

Figure 28. Schematic diagram of case model.

Table 7. Working conditions of the case.

Condition No.	Span Number	Damage Degree	Damage Position	Number of Damages
Condition 1	Two-span	No damage	NO	0
Condition 2	Two-span	Two-point 25% damage	One-span 1/4 position and two-span 3/4 position	2
Condition 3	Two-span	Two-point 25% damage	One-span position 50 mm away from the hinge support, two-span 3/4 position	2
Condition 4	Two-span	Two-point 25% damage	One-span 1/2 position and two-span 3/4 position	2
Condition 5	Two-span	Two-point 25% damage	Midspan position (damage width: 200 mm) and two-span 3/4 position	2
Condition 6	Two-span	Two-point 25% damage	Midspan position (damage width: 300 mm) and two-span 3/4 position	2
Condition 7	Two-span	Two-point 25% damage	Midspan position (damage width: 400 mm) and two-span 3/4 position	2

The inherent frequencies of the test beam at different orders under different conditions were measured through the abovementioned testing method, as listed in Table 8.

Table 8. Inherent frequency loss rates at different orders.

Order of Vibration Mode	Condition 1	Condition 2		Condition 3		Condition 4	
	Frequency (Hz)	Frequency (Hz)	Frequency Loss Rate %	Frequency (Hz)	Frequency Loss Rate %	Frequency (Hz)	Frequency Loss Rate %
1	7.2525	6.8123	6.07	7.0053	3.41	6.839	5.70
2	7.5042	7.0088	6.60	7.2162	3.84	7.00782	6.61
3	20.009	16.929	15.39	17.104	14.52	17.143	14.32
4	20.677	18.669	9.71	18.984	8.19	18.93	8.45
5	39.304	37.345	4.98	34.546	12.11	34.015	13.46
Order of Vibration Mode	**Condition 1**	**Condition 5**		**Condition 6**		**Condition 7**	
	Frequency (Hz)	**Frequency (Hz)**	**Frequency Loss Rate %**	**Frequency (Hz)**	**Frequency Loss Rate %**	**Frequency (Hz)**	**Frequency Loss Rate %**
1	7.2525	6.7894	6.39	6.7458	6.99	6.7252	7.27
2	7.5042	6.8559	8.64	6.8402	8.85	6.8388	8.87
3	20.009	17.128	14.40	17.01	15.00	16.77	16.18
4	20.677	18.991	8.15	18.775	9.20	18.518	10.44
5	39.304	34.015	13.46	33.265	15.36	33.29	15.30

Table 8 shows that the frequency loss rate of third-order vibration mode was higher as abovementioned. Meanwhile, by comparing the frequencies under Conditions 1, 4, 5, 6 and 7, we found that with the expansion of damage width, the frequency was not sensitive to the damage change at the same position.

The related displacement mode curves were directly plotted together to compare the displacement mode curves under Conditions 1 to 4, as shown in Figure 29.

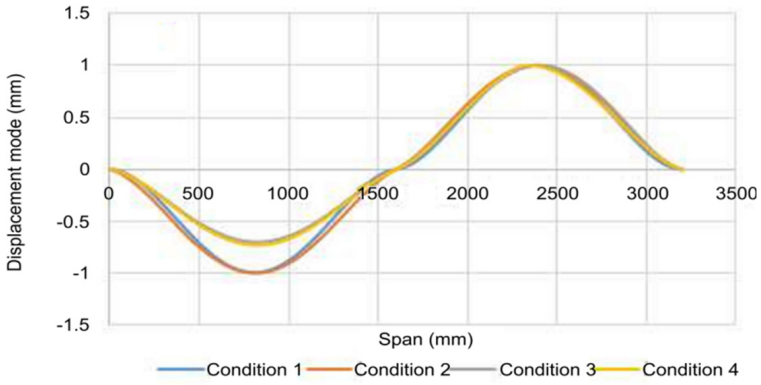

(**a**) Vibration mode curves under Conditions 1 to 4.

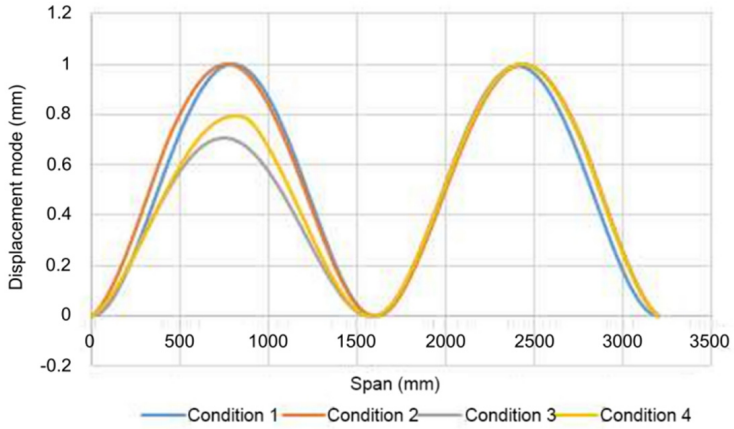

(**b**) Second-order vibration mode curves under Conditions 1 to 4.

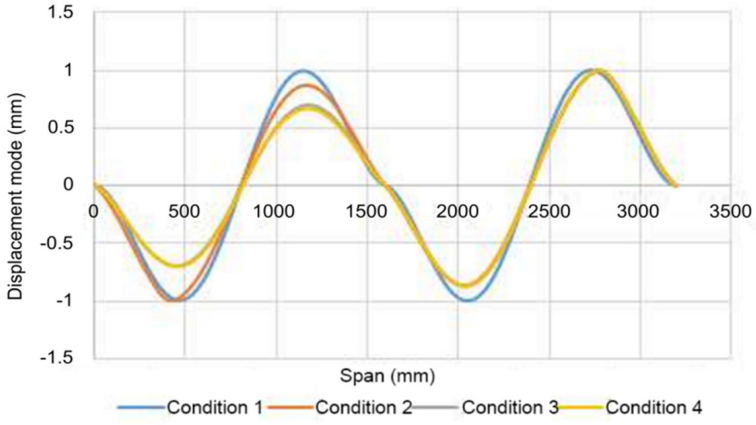

(**c**) Third-order vibration mode curves under Conditions 1 to 4.

Figure 29. *Cont*.

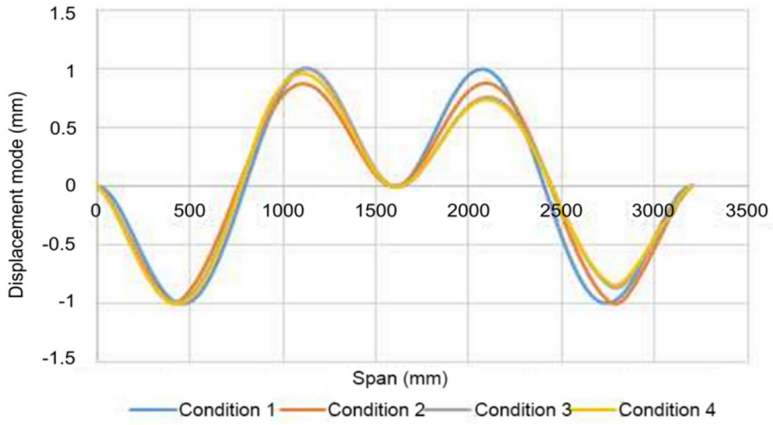

(**d**) Fourth-order vibration mode curves under Conditions 1 to 4.

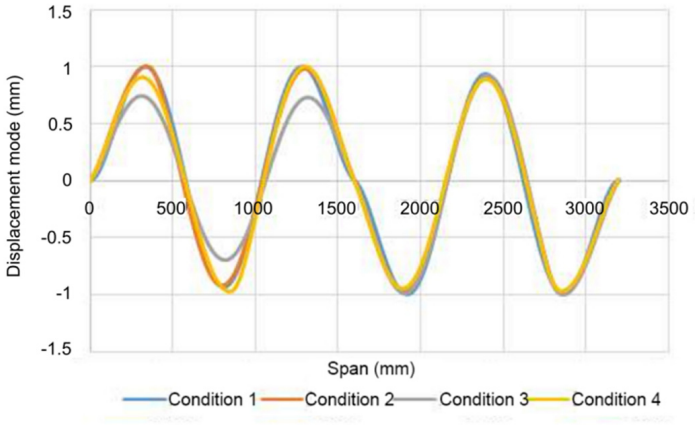

(**e**) Fifth-order vibration mode curves under Conditions 1 to 4.

Figure 29. First five orders of vibration mode curves under Conditions 1 to 4.

As with the working conditions of a single-span beam, the difference between displacement modes was not great, and the displacement difference only appeared at the damage position more or less. The images were approximately overlapped even if damages existed at the second span, which served as the control variable and the comparison span. Given that the difference value of displacement mode curves for the double-span continuous beam was approximately similar to that for the single-span beam, only the first-order derivative of the first-order mode was verified. To facilitate the comparison, the difference values of first-order vibration modes under different working conditions were plotted onto the same graph (Figure 30).

It can be observed from the above curves that the first-order derivative curve of first-order vibration mode difference was located at the midspan damage of the first span, and the fluctuation width of singularity increased with the increase in the damage width, indicating that the first-order derivative curve of first-order vibration mode difference is of particular reference value for identifying the damage scope.

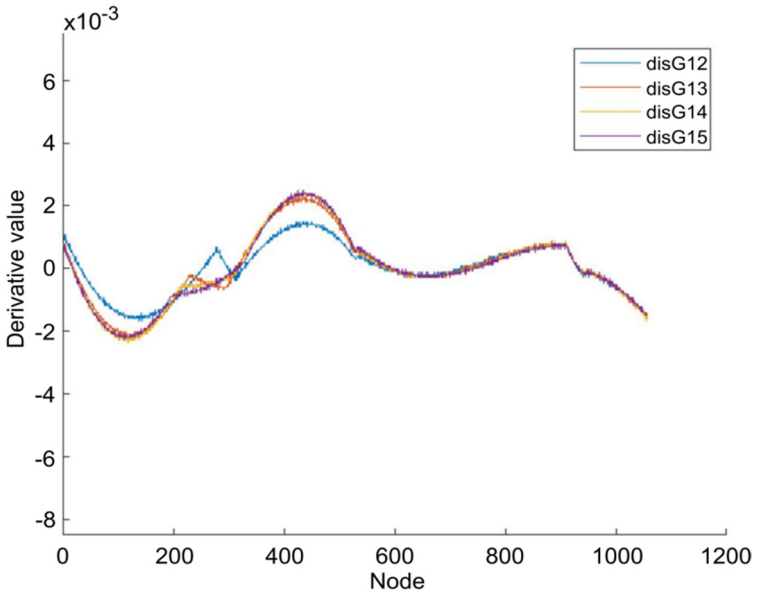

Figure 30. First-order derivatives of first-order mode differences under Conditions 1, 4, 5, 6 and 7.

4. Conclusions

In this study, a beam structure damage identification method was explored through finite element simulation and experiment from structural inherent frequency and displacement mode angles. Directed damages were created for the experimental beam and finite element model. It was discovered that the inherent structural frequency would be reduced in case of any damage, and the frequency loss rate of the third-order vibration mode was the maximum among the first five orders of vibration modes. Through these findings, whether the structure is damaged can be tentatively judged, but the damage position cannot be determined. The damage will affect the structural displacement mode, and the structural displacement will be aggravated at the damaged part. Therefore, the damage scope can be inferred, but the structural displacement mode difference, which is too small, can hardly be observed. The displacement mode difference was amplified by solving the derivatives of mode difference to solve this problem. Through comparing the first-order and second-order derivatives of the first five orders of displacement mode differences under different working conditions, the first-order derivative of the first-order vibration mode difference was considered the reference basis for the damage identification. This parameter is capable of sensitively identifying the rough damage position. However, the fluctuation trend will gradually be smooth when damage with great width is identified, and the damage scope cannot be accurately identified in the case of small data points. Besides, the identification effect on the damage close to the support is unsatisfactory. Defects still exist in this study. Only directed damages were assigned to the experimental beam, but the damage conditions are incredibly complicated in practical engineering. Moreover, the identification effect of the proposed method under unknown damage conditions remains unclear and should be explored in the future.

Author Contributions: Conceptualization, Y.Z., X.T., G.L. and F.L.; methodology, Y.Z., X.T., G.L., J.D., J.G. and F.L.; validation, Y.Z., X.T., G.L., J.D., J.G. and F.L.; formal analysis, Y.Z., X.T., G.L., J.D., J.G. and F.L.; investigation, Y.Z., X.T., G.L., J.D., J.G. and F.L.; resources, Y.Z., X.T., G.L., J.D., J.G. and F.L.; data curation, Y.Z., X.T., G.L., J.D., J.G. and F.L.; writing—original draft preparation, Y.Z., X.T., G.L., J.D., J.G. and F.L.; writing—review and editing, Y.Z., X.T., G.L., J.D., J.G. and F.L.; visualization, Y.Z., X.T., G.L., J.D., J.G. and F.L.; supervision, Y.Z., X.T., G.L., J.D., J.G. and F.L.; project administration, Y.Z., X.T., G.L., J.D., J.G. and F.L.; funding acquisition, Y.Z., X.T., G.L., J.D., J.G. and F.L. All authors have read and agreed to the published version of the manuscript.

Funding: This research was supported by the Natural Science Foundation of Beijing, China (Grant No. 82020120), and the National College Students' Innovation and Entrepreneurship Training Project (Grant No. 202010016018 and Grant No. 202110016019).

Institutional Review Board Statement: Not applicable.

Informed Consent Statement: Not applicable.

Data Availability Statement: All the data can be requested from the corresponding author upon reasonable request.

Conflicts of Interest: The authors declare no conflict of interest.

References

1. Wang, Y. Bridge Damage Identification Based on the Change of Inherent Frequency. Ph.D. Thesis, East China Jiaotong University, Jiangxi, China, 2012.
2. Pandey, A.K.; Biswas, M. Experimental verification of flexibility difference method for locating damage in structures. *J. Sound Vib.* **1955**, *184*, 311–328. [CrossRef]
3. Hearn, G.; Testa, R.B. Modal analysis for damage detection in structures. *J. Struct. Eng.* **1991**, *171*, 3042–3063. [CrossRef]
4. Ramanjaneyulu, K.; Srinivas, V.; Sasmal, S.; Jeyasehar, C.A. Damage identification based on vibration data. *Int. J. Forensic Eng.* **2013**, *1*, 209–226. [CrossRef]
5. Weng, J.C. Study on Damage Identification of Simple Supported-to-Continuous Bridge Based on Curvature Mode Theory. Master's Thesis, Southwest Jiaotong University, Chengdu, China, 2013.
6. Hu, Y.C. Study of Beam Bridge Damage Identification Based on Structural Dynamic Characteristics. Ph.D. Thesis, Wuhan University of Technology, Wuhan, China, 2014.
7. Wu, Q.Y. Study of Beam Structure Damage Identification Based on Dynamic Characteristics. Ph.D. Thesis, Wuhan University of Technology, Wuhan, China, 2019.
8. Liu, C.; Wu, D.; Li, Y.; Du, Y. Large-scale pavement roughness measurements with vehicle crowdsourced data using semi-supervised learning. *Transp. Res. Part C Emerg. Technol.* **2021**, *125*, 103048. [CrossRef]
9. Fang, Q.; Wang, G.; Yu, F.; Du, J. Analytical algorithm for longitudinal deformation profile of a deep tunnel. *J. Rock Mech. Geotech. Eng.* **2021**, *13*, 845–854. [CrossRef]
10. Lu, N.; Wang, H.; Wang, K.; Liu, Y. Maximum Probabilistic and Dynamic Traffic Load Effects on Short-to-Medium Span Bridges. *Comput. Modeling Eng. Sci.* **2021**, *127*, 345–360. [CrossRef]
11. Luo, Y.; Zheng, H.; Zhang, H.; Liu, Y. Fatigue reliability evaluation of aging prestressed concrete bridge accounting for stochastic traffic loading and resistance degradation. *Adv. Struct. Eng.* **2021**, *24*, 3021–3029. [CrossRef]
12. Xiao, X.; Bu, G.; Ou, Z.; Li, Z. Nonlinear in-plane instability of the confined FGP arches with nanocomposites reinforcement under radially-directed uniform pressure. *Eng. Struct.* **2022**, *252*, 113670. [CrossRef]
13. Zhang, H.; Liu, Y.; Deng, Y. Temperature gradient modeling of a steel box-girder suspension bridge using Copulas probabilistic method and field monitoring. *Adv. Struct. Eng.* **2021**, *24*, 947–961. [CrossRef]
14. Su, B.J. Study of Beam Structure Damage Identification Based on Dynamic Characteristics. Ph.D. Thesis, Xiangtan University, Xiangtan, China, 2018.
15. Jia, C. Study of Structural Damage Identification Method Based on Dynamic Characteristics. Ph.D. Thesis, Jilin Jianzhu University, Changchun, China, 2017.
16. Wei, T. Study on Damage Identification of Steel Truss Bridge Based on Inherent Frequency and Curvature Mode. Ph.D. Thesis, Xihua University, Chengdu, China, 2018.
17. Lian, X. Study of Damage Identification Based on Dynamic Characteristics of Bridge. Ph.D. Thesis, North China University of Water Resources and Electric Power, Zhengzhou, China, 2018.
18. Zhao, Y.P. Study on Damage Identification of Concrete Simple-Supported Beam Bridge Based on Dynamic and Acoustic Characteristics. Ph.D. Thesis, Northeast Forestry University, Harbin, China, 2019.
19. Mousavi, A.A.; Zhang, C.; Masri, S.F.; Gholipour, G. Damage detection and localization of a steel truss bridge model subjected to impact and white noise excitations using empirical wavelet transform neural network approach. *Measurement* **2021**, *185*, 110060. [CrossRef]
20. Jahangir, H.; Hasani, H.; Esfahani, M.R. Wavelet-based damage localization and severity estimation of experimental RC beams subjected to gradual static bending tests. *Structures* **2021**, *34*, 3055–3069. [CrossRef]
21. Kordestani, H.; Zhang, C.; Shadabfar, M. Beam damage detection under a moving load using random decrement technique and Savitzky–Golay filter. *Sensors* **2020**, *20*, 243. [CrossRef] [PubMed]